Towards Using Tire-Road Contact Stresses in Pavement Design and Analysis

M. De Beer*, J. W. Maina, Y. van Rensburg, J. M. Greben

mbeer@csir.co.za

CSIR Built Environment

P O Box 395

Pretoria

0001

South Africa

Presented at the

September 2011

Meeting of the Tire Society

*Presenter / Corresponding Author

REFERENCE: M. De Beer, J. W. Maina, Y. van Rensburg and J. Greben "Towards Using Tire-Road Contact Stresses in Pavement Design and Analysis," submitted for presentation at the 2011 Tire Society meeting, and for consideration for publication in the journal *Tire Science and Technology*.

ABSTRACT: Optimization of road pavement design, especially towards the surface of the pavement, requires a more rational approach to modeling of truck tire-road contact stresses. Various road surfacing failures are given in this paper as examples, and it is shown that the traditional civil engineering tire model represented by a single uniformly distributed vertical contact stress of circular shape is inadequate to explain this type of surface failure. This paper therefore discusses the direct measurement of three-dimensional (3D) tire pavement contact stresses using a flatbed sensor system referred to as the "Stress-In-Motion" (SIM) system. The SIM system (or device) consists of multiple conically shaped steel pins, as well as an array of instrumented sensors based on strain gauge technology. The test surface is textured with skid resistance approaching that of a dry asphalt layer. Full-scale truck tires have been tested since the mid-1990s and experience shows that 3D tire contact stresses are non-uniform and the footprint is often not of circular shape. It was found that especially the vertical shape of contact stress distribution changes, mainly as a function of tire loading. In overloaded/underinflated cases, vertical contact stresses maximize towards the edges of the tire contact patch. Higher inflation pressures at lower loads, on the other hand, result in maximum vertical stresses towards the center portion of the tire contact patch. These differences in shape and magnitude need to be incorporated into modern road pavement design. Four different tire models were used to represent a single tire type in order to demonstrate its effect on road pavement response of a typical South African pavement structure. Only applied vertical stress was used for the analyses. It was found that road surface layer life can reduce by as much as 94 percent as a result of simply using a different tire model on the same pavement structure.

KEYWORDS: Tire, Contact, Tire-Road, Stress, Force, Measurement, Load, Patch, Pavement, Design, Strain Energy of Distortion (SED).

Road Pavements – Some Aspects of Surface Failure

Road pavements worldwide are one of the most important infrastructure elements which should be maintained in good to excellent condition in order to service the economy of any progressive nation. Most of the time, however, road pavement failures initiate within the pavement structural or subgrade layers long before they are visible on the surface of the pavement. There are mainly two basic classes of pavement failures, i.e., traffic-associated and non-traffic-associated failures. Non-traffic-associated failures are those associated with the environment, mainly through variations in temperature and water (moisture) over time. Traffic-associated failures are due to tire-road contact, where tire (or vehicle) loading is transferred to the structural layers of the pavement, which is usually covered with a functional surfacing layer. However, the importance of the structural behavior of the final layer of a paved road system should not be underestimated, both from a safety perspective and because it serves as a protective layer for the structural layers of the pavement system. Meyers *et al.* (1999, 2001) [22], [23], Novak *et al.* (2003) [24], and Roque *et al.*, (1998, 2000) [28], [29] all indicated potential road failures (rutting/cracking) originating at the near surface of the pavement due to, among others, the Poisson's effect under the ribs of pneumatic truck tires causing some strains in the near surface of the pavement next to the tire edge. Further research on tire-induced surface shear stresses on road surfaces was also done by Priest and Timm in 2006 [27], as well as Soon *et al.* in 2003 [30]. Perdomo and Nokes indicated in 1993 [26] that peak tensile stresses may occur in a shallower part of the surface layer.

The aim of this paper is to discuss aspects of measured tire-road contact stresses (in three dimensions (3D)) within the tire contact patch (footprint) of typical truck tires. It is shown by relatively simple tire-pavement contact analysis that higher (or different) contact stresses could potentially result in an increased potential for road pavement failures, mostly visible within the final surfacing layer, or near the surface of pavement layers.

Observations of Road Pavement Failures

In South Africa, most flexible paved road pavement structures consist of a relatively thin asphalt surfacing layer covering the base layer, which is often a 150 mm high-quality unbound crushed rock material, compacted to a solid density of 86 to 88 percent material specification [2]. The thickness of these asphalt surfacing layers varies between 25 mm and 30 mm, and the vast majority of primary roads are covered with an asphalt seal layer (chip stones, or chip seal), with a thickness of approximately 12 mm to 20 mm (see FIG. 1). In the wetter coastal regions of South Africa, the crushed stone layer is replaced by an asphalt base layer of approximately 120 mm or more. It is therefore of critical importance to quantify and also improve the understanding of the actual tire-road contact stresses (or forces), and, if possible, also to quantify them in 3D, in order to optimize road layer "life" (or bearing capacity) by means of effective road design and associated maintenance schedules, often with limited budgets and resources.

FIG. 1. Aerial view of a high-quality thinly surfaced divided freeway near Pretoria, South Africa.

The failures of these functional surfacing layers include both plastic deformation such as "rutting" (see FIG. 2), and/or shoving/horizontal plastic flow (see FIG. 3), fatigue cracking (see FIG. 4), delamination (see FIG. 5), disintegration (see FIG. 6), the

formation of potholes (see FIG. 7), and subsurface rutting often with standing water in the wheel paths (see FIG. 8) during rain. FIG. 9 shows an example of a substandard base layer, causing the typical ”wiggling yellow line” indicative of shear failure in the unbound base layer. Most of these failures are related to tire-road interaction and are therefore considered “traffic associated”. In this paper it is postulated that an improved understanding of the 3D tire-road interaction forces (or contact stresses) could serve as a sound platform for the formulation of improved pavement design rules. The traditional assumption of one-dimensional (1D) uniformly distributed tire loading on a circular shape for pavement design as discussed by Huang in 1993 [18], and Yoder and Witczak in 1975 [35] is therefore questioned.

FIG. 2. Plastic deformation (or rutting/shoving) within the thin asphalt surfacing layer. Note the six lanes of rutting (left and right sides) owing to tire loading combined with poor asphalt mix.

FIG. 3. Horizontal plastic deformation (or rutting/shoving) within the thin asphalt surfacing layer at an intersection. Note the planar backwards deformation depicted by the white lane marking owing to the tractive acceleration forces of tires towards the right of the picture.

FIG. 4. Fatigue (alligator) cracking of a old and brittle thin surface seal. Note fatigue cracking with some signs of white coloring (pumping of fines) in insert.

FIG. 5. Delamination of the asphalt surfacing layer from the lower layer.

FIG. 6. Surface disintegration in the asphalt surface seal of a low-volume road.

FIG. 7. Typical pothole with water in a thinly surfaced road.

FIG. 8. Standing water on pavement with wheel path rutting causing a safety (hydroplaning) hazard.

FIG. 9. "Wiggling yellow line" owing to shear failure in a substandard (or wet) granular base layer.

Tire Inflation Pressure of Heavy Vehicles

A major assumption in road pavement design is that the vertical tire-pavement contact stress is assumed to be equal to the tire inflation pressure, and to be of circular and uniform shape [18], [35]. With regard to tire inflation pressure trends, several studies since 1974 have shown an increase in the inflation pressure of the tires of heavy vehicles. A comparison of the data from 1974 with those of 1995 shows that there was a 20 percent increase in average inflation pressure over 20 years in South Africa (see FIG. 10), apparently owing to improved truck tire design (cross-ply to radial) to carry higher loads and longer tire life.

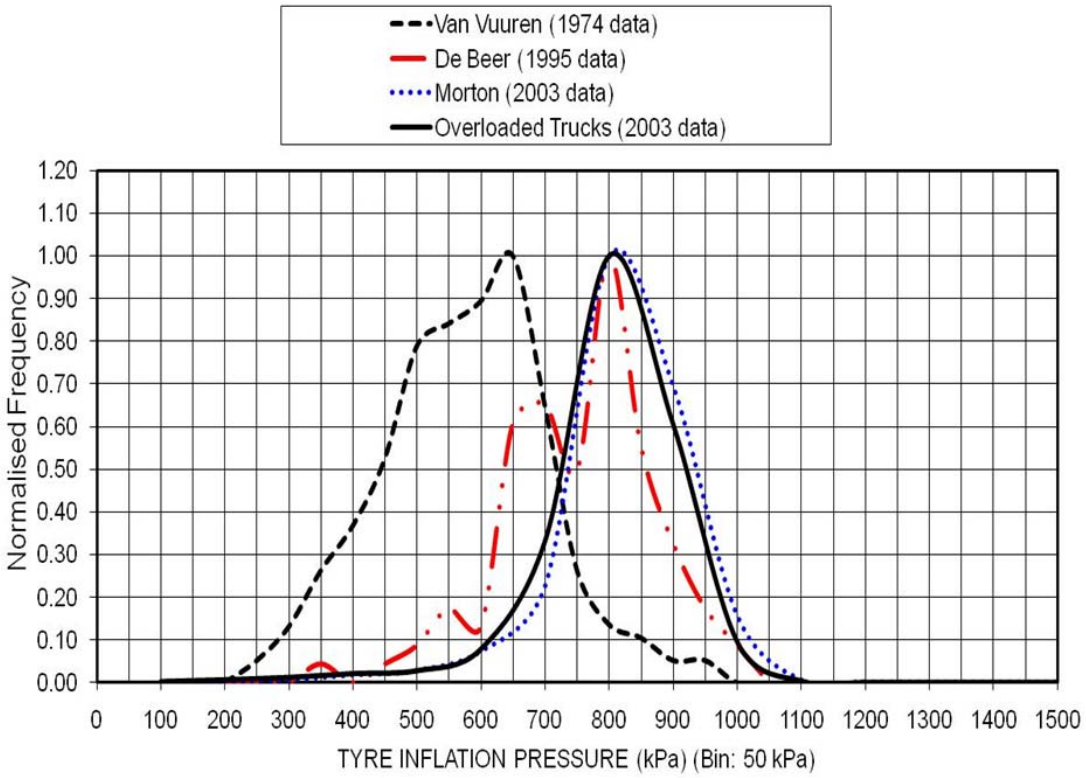

FIG. 10. Distribution of tire inflation pressure of heavy vehicles in South Africa since 1974. For details in legend see [4].

The data in FIG. 10 show an increase from an average inflation pressure (cold) of 633 kPa in 1974 to 733 kPa in 1995, and that the pressures are currently approaching an average of 800 kPa (116 psi), with maximum pressures exceeding 1,000 kPa (145 psi). FIG. 11 illustrates the results of a more recent study in which a difference in tire inflation pressure was observed between steering tires and trailing tires of approximately 100 kPa (14.5 psi) (cold). The average inflation pressure was approximately 900 kPa (131 psi) for the steering tires, and 800 kPa (116 psi) for the trailing tires of a selection of heavy vehicles.

It should be noted that back in the 1970s Van Vuuren [34] recommended a value of 520 kPa (75.4 psi) for circular uniform contact stress for pavement design in South Africa.

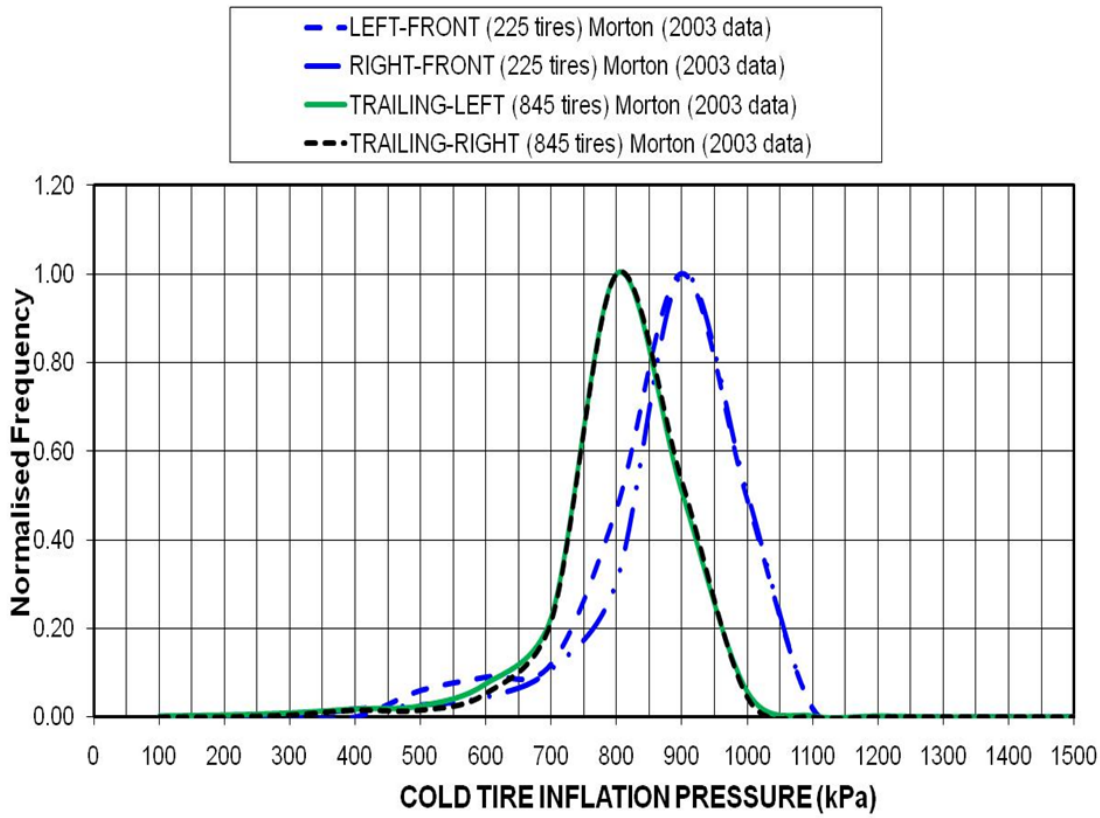

FIG. 11. Tire inflation pressure differences between the steering and trailing tires of a selected group of heavy vehicles in South Africa in 2003 (from [12]).

Tire contact stress measurements

Based on the increasing trend of truck tire inflation pressures found in South Africa, in association with numerous road surface failures (also demonstrated by Heavy Vehicle Simulator (HVS) accelerated pavement testing and research) [16], [31], it was decided to further study tire contact stress measurements, which dated back to 1965 [1]. During the 1990s a rigid flatbed device with a textured surface was successfully developed and used to measure the tire-pavement contact stresses of a range of pneumatic truck tires. The single pad of the device, referred to as the "Stress-In-Motion" (SIM) device (referred to earlier as Vehicle Road Surface Transducer Array, or VRSPTA [5], [6], [7]), is shown in FIG. 12 (single SIM pad), and FIG. 13 (dual SIM pad configuration). The SIM system is modular and a test bed configuration of up to 2,100 mm wide is possible with this setup (more information is available in a fact sheet on the following website at

http://www.csir.co.za/Built_environment/brochures.html [36]. For controlled tire loading and tire inflation pressure the HVS was used for tire-pavement contact stress measurements in association with the SIM device. The first typical SIM data were published by De Beer in 1996 [5], and a comprehensive summary was presented in 1997 [7]. This was followed by several presentations relating SIM data with mechanistic analyses of road pavements in 1999 [8], 2002 [9], 2004 [10], [11], 2006 [12], and 2008 [13].

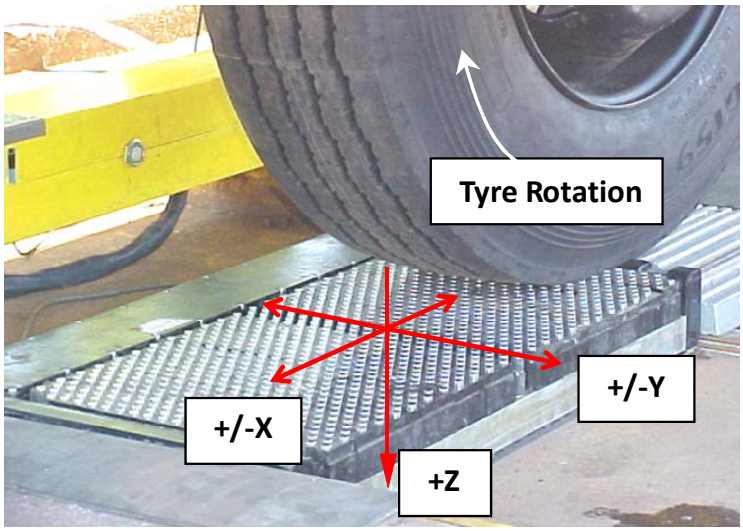

FIG. 12. Flat bed Stress-In-Motion (SIM) device with Society of Automotive Engineering (SAE) coordinate system used in this study for the measurements of 3D tire contact force (or stress) conditions inside the tire contact patch of a slow-rolling pneumatic tire (fitted on the Heavy Vehicle Simulator – HVS).

FIG. 13. Dual SIM device under tire loading using the Heavy Vehicle Simulator (HVS).

Typical Tire Contact Stress Results from the SIM System

The SIM device was developed mainly for the measurement of slow-moving pneumatic truck tires (speed approx. 5 km/h). A single SIM pad consists of 21 instrumented conically shaped hollow cylindrical pins in a linear configuration across the SIM device. The surface contact area of the pins is approx. 94 mm^2 (diameter of 9.7 mm) at a fixed lateral resolution of 17 mm c/c. Each pin consist of a 5-axial load cell based on traditional strain gauge technology, calibrated against a high-precision miniature load cell, which in turn is calibrated against dead weight [5], [6], [7]. In the longitudinal direction the resolution is a function of the test speed (V in m/s) of the tire divided by the sampling rate (usually 1,000 Hz per channel). For typical HVS testing with the SIM device, the longitudinal increment is approx. 0.3 mm. The fore and aft sections of the SIM pad (which is 350 mm wide and 750 mm in length) also consist of a number of conically shaped supporting pins (total more than 1,000) of similar shape and size to the instrumented pins. This configuration results in a textured measuring surface with friction values approximating those of a dry asphalt surface [7], which means the tire is approaching the textured surface of the SIM device (or measuring pad). Measurement is

made in the center portion of the SIM pad after the front part of the tire contact patch has been “conditioned” by the textured surface, after which the aft part of the contact patch is measured. A 3D contact stress pattern is obtained in one measurement cycle.

It should be noted that partial contact of instrumented SIM pins on rib or element edges does occur with this system. The instrumented pins capture the components of a vector force in the three directions (X, Y, Z) whenever there is contact with rubber, instantaneously. In such a case, there is no specialized treatment of data necessary, but additional passes could provide improvement of the definition of the forces/stresses at the rib edges (where there is partial contact), especially when the tread pattern varies along the tire patch. Further, non-ribbed tire designs (lug pattern) can be measured with the SIM device. For this case, there can be a difference in the vertical pressure trace (leading footprint edge to trailing footprint edge), depending on where the sensor (or instrumented) pin contacts the individual tread lug (leading lug edge vs trailing lug edge). Non-ribbed lug pattern tire design requires multiple passes in order to capture the variation of contact forces/stresses along the length of the tire patch. In one example, a sinusoidal pattern of total loading was observed, discussed in De Beer and Fisher in 1997 [6].

Typical contact stress results under a standard dual 11xR22.5 tire load of 40 kN and inflation pressure of 520 kPa (typical standard axle of 80 kN). Examples of measured vertical (+Z), lateral (+/- Y) and longitudinal (+/- X) contact stresses, are illustrated in FIG. 14, FIG. 15 and FIG. 16, respectively. Note that higher test speeds can be achieved with the SIM system, and are dependent mainly on the data acquisition system. The natural frequency of the instrumented pins (or sensors) is approximately 3,700 Hz. A typical truck tire, with length (L) with the tire contact patch of 250 mm traveling at a speed (V) of 80 km/h, will result in a total data count of approx. [250 mm]/[80,000 m/(60 x 60)] = 11, with increments between the data points of 22.2 mm. However, most of the measurements were made at a speed of approx. 0,3 m/s, resulting in data counts varying between 200 and 1,000, depending on the length of the tire contact patch (L), the speed (V) and the sampling frequency (f). Currently the sampling frequency is 1,000 Hz.

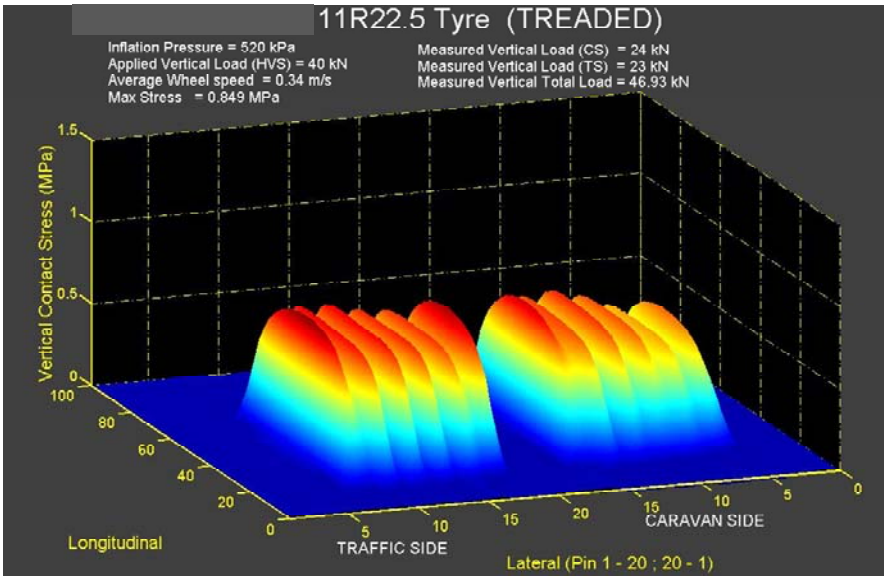

FIG. 14. Typical vertical (Z) contact stress pattern of a 11xR22.5 dual tire configuration with total tire load of 40 kN, and 520 kPa inflation pressure. Note that a maximum contact stress of approx. 849 kPa was measured on the edge of the left tire in this illustration.

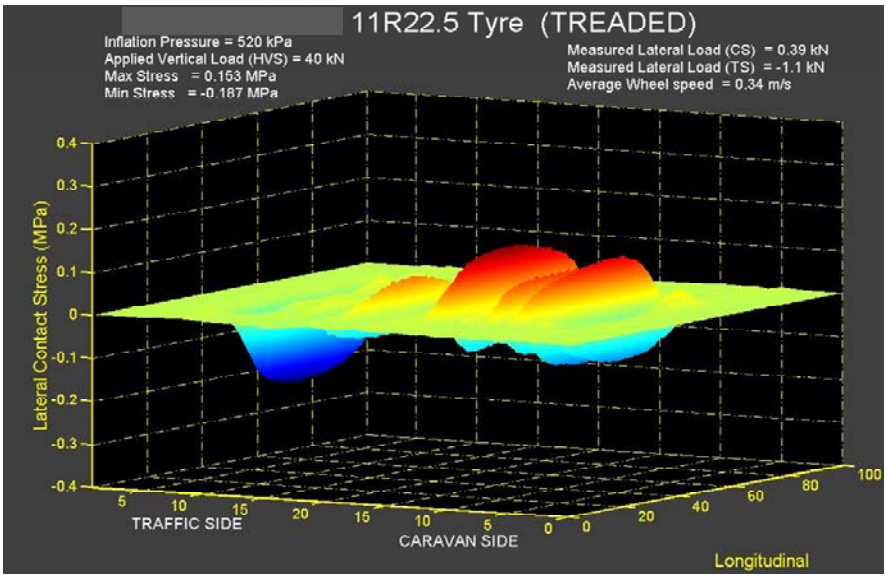

FIG. 15. Typical lateral (+/- Y) contact stress pattern of a 11xR22.5 dual tire configuration with total tire load of 40 kN, and 520 kPa inflation pressure. Note that a maximum contact stress of approx. 187 kPa was measured on the edge of the right tire in this illustration.

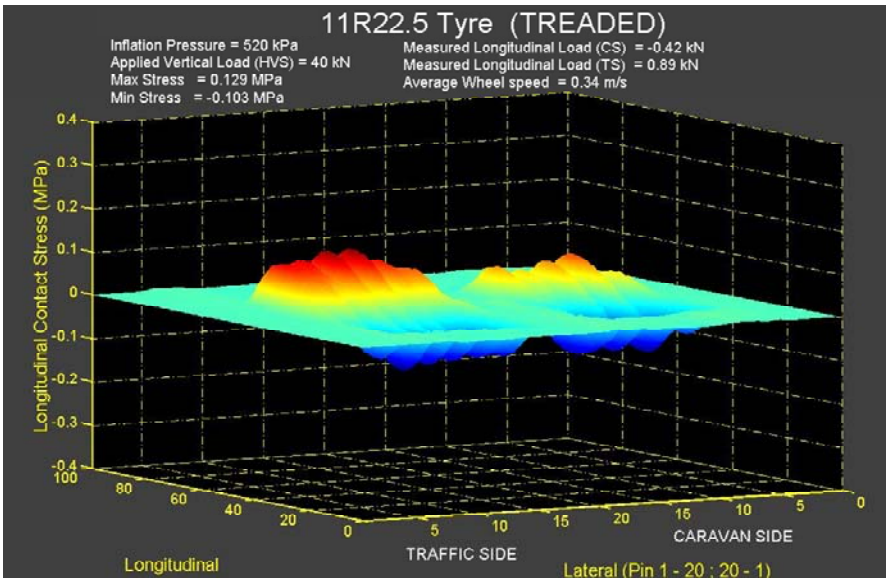

FIG. 16. Typical longitudinal (+/- X) contact stress pattern of a 11xR22.5 dual tire configuration with total tire load of 40 kN, and 520 kPa inflation pressure. Note that a maximum contact stress of approx. 129 kPa was measured on the fore end of the left tire in this illustration.

In FIG. 17 and FIG. 18 some measured tire test results are shown with HVS loading at 40 kN/800 kPa, resulting in "n-shape" rutting, and an overloaded/underinflated case of 80 kN/420 kPa, resulting in "m-shape" rutting. The resulting shapes of the road surface rutting mimicking the shape of the "n-shape" and "m-shape" vertical tire contact stress (Z), respectively. In FIG. 19, typical tire footprints ("collectively referred to as tire "fingerprint") of the vertical contact stress variation with tire loading (vertical scale from 15 kN to 50 kN) and with variation in tire inflation pressure (horizontal axis from 520 kPa to 800 kPa) is illustrated. Similar data can be presented for the measured +/- lateral and +/- longitudinal contact stresses. FIG. 19 illustrates the effect of tire loading at constant tire inflation pressure and clearly shows the changes in the contact stress pattern from a relatively light load, where the maximum stress is towards the tire center (typical bell or "n-shape"), to the typical dual bell, or "m-shape", where the load is carried mostly by the tire sidewalls, showing the highest contact stresses at the tire edges, as originally described in 1997 [7]. The ideal (and often rated load/inflation pressure condition) is shown here at a tire load of 20 kN and a rated inflation pressure of 720 kPa. In the latter

case a more uniform pressure (or vertical contact stress) distribution is observed (see FIG. 19).

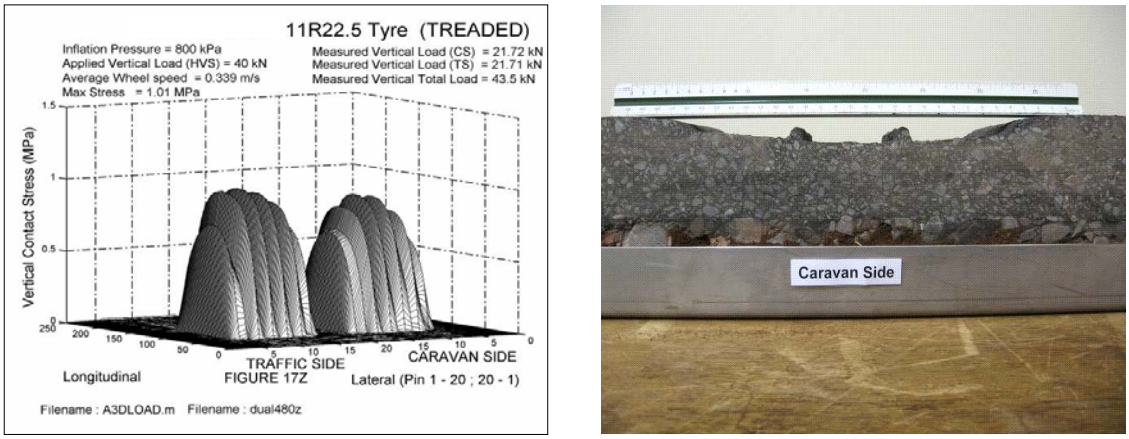

FIG. 17. Heavy Vehicle Simulator (HVS) tire loading of 40 kN, and inflation pressure of 800 kPa (with typical "n-shape" vertical stress distribution), resulting in typical "n-shape" plastic deformation in a thin asphalt surfacing layer – only one HVS tire traffic lane is shown here [21]

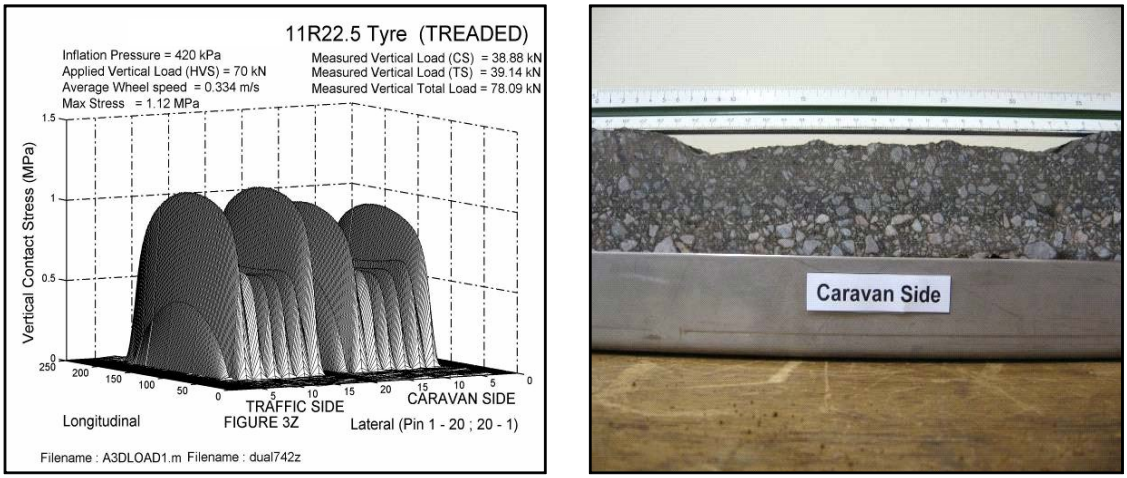

FIG. 18. Heavy Vehicle Simulator (HVS) tire (over) loading of 80 kN, and inflation pressure of 420 kPa (with typical "m-shape" vertical stress distribution), resulting in typical "m-shape" plastic deformation in a thin asphalt surfacing layer – only one tire HVS traffic lane is shown here [21]

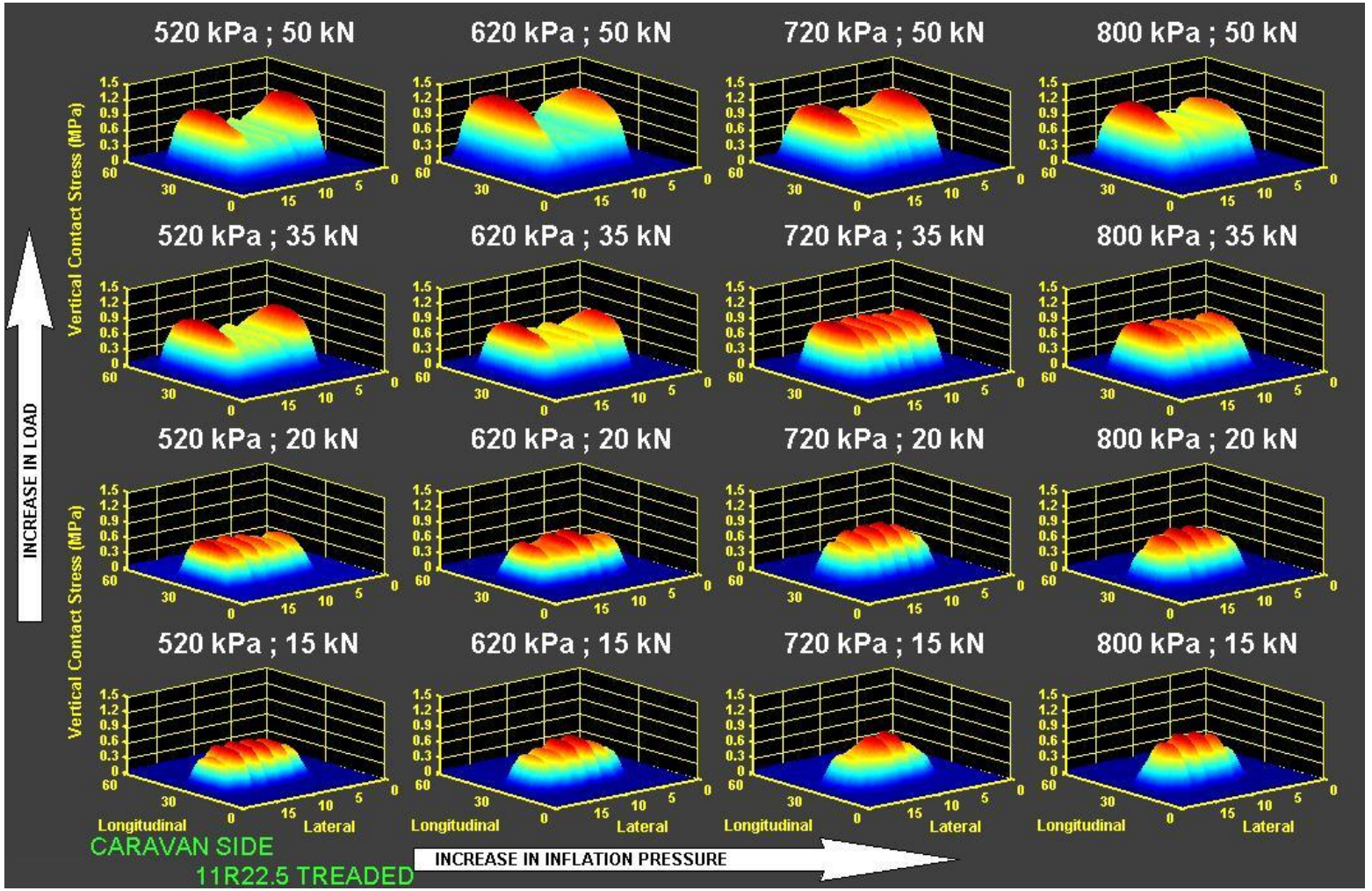

FIG. 19. Typical tire "fingerprint" of the vertical contact stress variation with tire loading (vertical scale from 15 to 50 kN) and with variation in tire inflation pressure (horizontal axis from 520 kPa to 800 kPa). Tire type 11xR22.5 with tread.

SIM Field Testing next to a National Freeway in South Africa

During 2003, a special study was conducted in which a selection of real truck traffic was diverted over a quad SIM system at the relatively slow speed of ~ 5 km/h. The test configuration is illustrated in FIG. 20. During this test series lasting for a period of six weeks, a total of about 2,900 heavy vehicles, representing approximately 45,000 tires, were measured with the SIM system [12], [13]. In FIG. 21 a typical vertical contact stress footprint of a 7-axle heavy vehicle (with 22 tires) captured with the SIM system in 2003 is illustrated. Note the non-uniformity of especially the tires on the steering axle, as well as the tires on drive axle number 3.

FIG. 20. Typical field configuration during a special test series with a quad SIM system conducted in 2003 in South Africa at the Heidelberg Traffic Control Center.

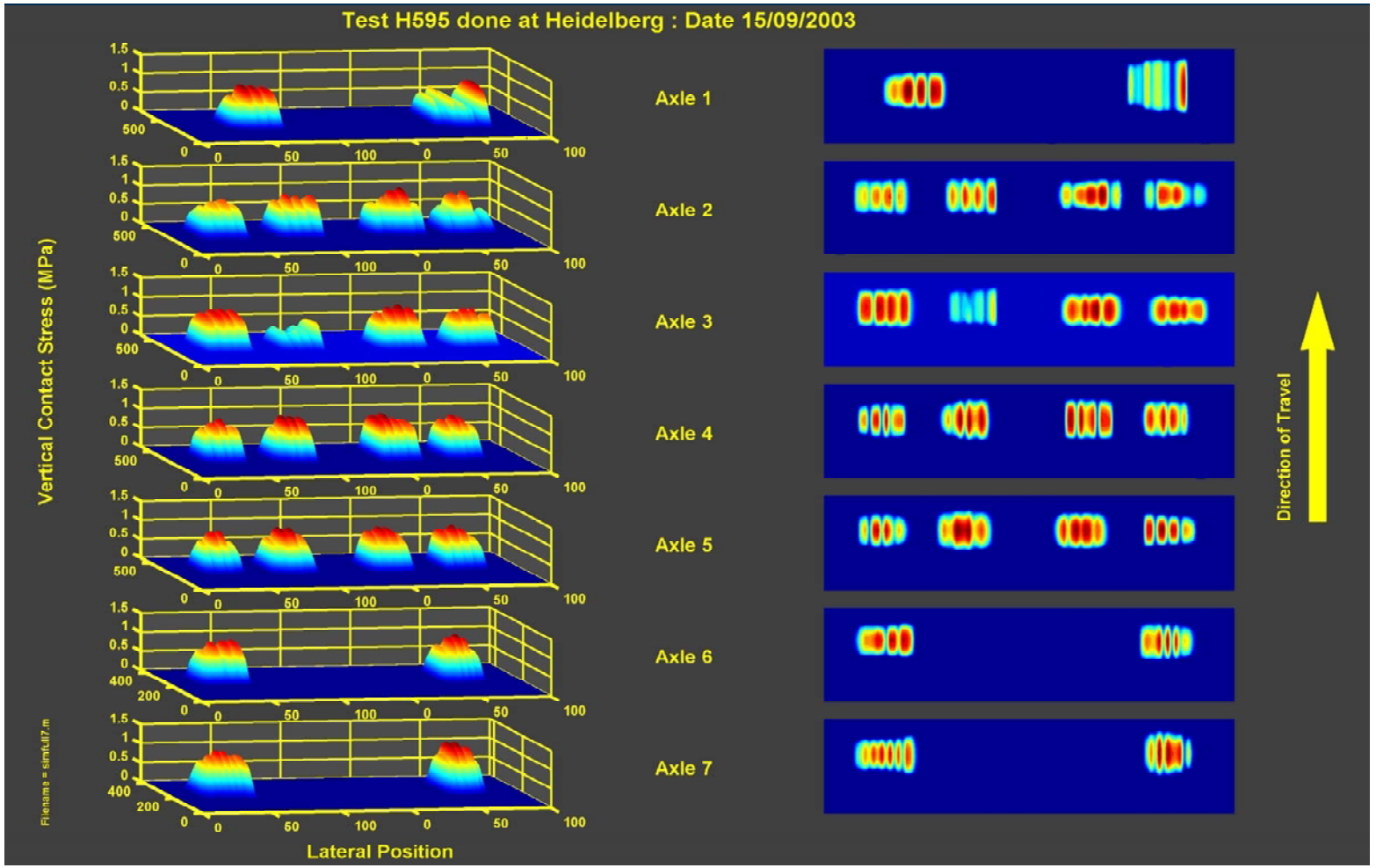

FIG. 21. Typical vertical contact stress footprint of a 7-axle heavy vehicle (22 tires) captured with the SIM system in 2003. Note the poor vehicle maintenance visible from the tire footprints.

Rolling Resistance

Although the SIM system was developed mainly to get an indication of 3D tire-road contact force (or stress) distributions across the tire contact patch for the purposes of improved road pavement design, closer inspection of the data of a 315/80 R22.5 tire showed some promise for estimating a "quasi-static" rolling resistance force (SRRf) on a textured measuring surface. Provisional data of three tire loading cases were extracted and are shown in FIG. 22. The figure indicates the measured total *resultant* longitudinal force (i.e., SRRf) during SIM measurement on the sample tire, as a function of vertical tire loading on the horizontal axis.

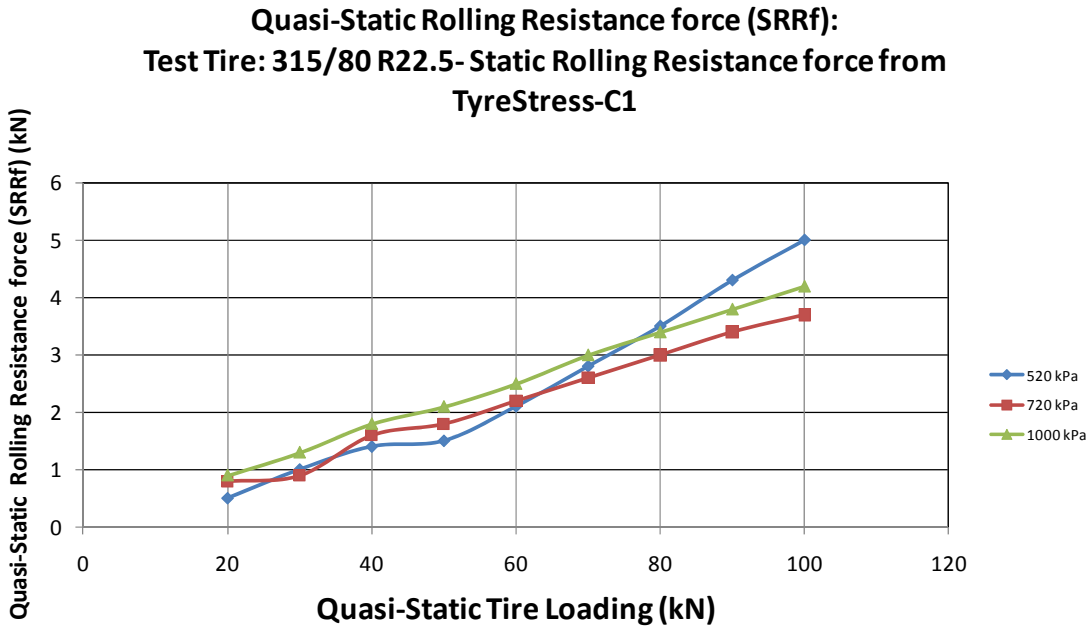

FIG. 22. "Quasi-static" rolling resistance force (SRRf) data on a textured measuring surface (SIM) for three tire inflation pressure cases of a 315/80 R22.5 tire at different vertical tire loading (F_z) levels.

TABLE 1. Quasi-Static Rolling Resistance coefficient (f_x)

	Quasi-Static Rolling resistance coefficient, f_x		
Static tire loading (kN), Fz	**520 kPa**	**720 kPa**	**1000 kPa**
20	0.025	0.040	0.045
30	0.033	0.030	0.043
40	0.035	0.040	0.045
50	0.030	0.036	0.042
60	0.035	0.037	0.042
70	0.040	0.037	0.043
80	0.044	0.038	0.043
90	0.048	0.038	0.042
100	0.050	0.037	0.042
Average	0.038	0.037	0.043
Standard deviation	0.008	0.003	0.001
Coefficient of Variation (CoV) (%)	21.94	7.95	2.94

In TABLE 1 the quasi-static rolling resistance coefficient *(f_x)* is given for the data illustrated in FIG. 22. Here f_x = *SRRf/Fz, representing normalized coefficients*, in terms of the classical definition of rolling resistance given by Gillespie [17]. On average, the highest f_x was found to be at a tire inflation pressure of 1,000 kPa, but the highest value was obtained at the lowest inflation pressure at 0.05 (which is comparable to values reported by Gillespie [17] for Heavy trucks). Note that this case also yielded the highest range in values (and CoV) as a function of vertical load, F_z. The results in FIG. 22, and TABLE 1 reports relatively higher rolling resistances at tire loads lower than 70 kN for the tire inflation pressure at 1,000 kPa, and is somewhat against conventional wisdom where higher tire pressures normally result in lower rolling resistance for hard surfaces, as also discussed by Gillespie [17]. However, further work on a wider range of tire data is needed to assess whether this procedure (and hence the method of measurement used in this paper on a textured measuring surface), could indeed be used to measure the rolling resistance of tires, comparable to conventional experiences.

The *preliminary* findings for the SIM measured data on a 315/80 R22.5 tire for slow-moving (< 10 km/h) free-rolling conditions include:

- There was a linear increase in SRRf with increased vertical tire loading at a rate of:
  - ~ 3 kN per 80 kN @ 750 kPa to 1,000 kPa to
  - ~ 4 kN per 80 kN @ 520 kPa cold inflation pressure.
- There was an increase in SRRf with increased loading and decreased inflation pressure (see 520 kPa result).
- The highest average rolling resistance coefficient (f_x = 0.043) was obtained at an inflation pressure of 1,000 kPa.
- The highest single value of the rolling resistance coefficient (f_x = 0.050) was obtained at the lowest inflation pressure (520 kPa) at the highest load investigated here. This case also resulted in the highest range of coefficients (f_x = 0.025 to 0.050), compared with those at inflation pressures at 720 kPa and 1,000 kPa. See TABLE 1.

The above data should be confirmed through more research on a wider range of tires and a wider range of operating conditions with the aid of the SIM system.

Road Pavement Analyses – A Simplistic Evaluation

In FIG. 23 a schematic is shown defining a multilayer road pavement structural design problem with "real" tire loading. The figure is self-explanatory. "Real tire loading" is defined here as that measured with the SIM system, as opposed to the general civil engineering assumption of a uniformly distributed vertical loading/stress of circular shape for the tire loading. This problem was also addressed by the development of the first worldwide tire/pavement contact-stress model based on artificial neural networks by El-Gindy and Lewis in 2001 [14], as well as by a study by Fernando *et al.* in 2006 [15], also based on SIM tire contact loading/stress measurements. For the present study, pavement analyses were done using the normal linear elastic multilayer analysis (LEA) approach

[18], with measured vertical loading/stress as input, using four different tire models. Note that since stresses are not required to be continuous in a displacement assumed finite element analysis (FEA), it is difficult to compute stresses accurately in the neighborhood of inter-element boundaries in FEA. Also in the case of FEA, the domain of analysis is finite contrary to the multilayered elastic systems (LEA) which contain a semi-infinite half space. Although analytical solution of multilayered elastic systems is also known to lose computational accuracy close to the surface where the load acts, this research has taken a special care to retain computational accuracy in the vicinity of load boundaries. Here, double exponential quadrature, discussed by Ooura and Mori in 1991 [25], has been utilized together with Richardson's extrapolation. Therefore, in this research, LEA was used in order to accurately determine strain-energy-of-distortion (SED) in the neighborhood of the tire (contact stress)-pavement interface.

Tire Models Used for Pavement Analyses in this Study

The four tire models used for pavement analyses in this study are:

- **Tire Model 1:** Assumed vertical loading of 20 kN and uniformly distributed vertical contact stress of 520 kPa of circular shape (i.e., disk) without restriction on the diameter of the disk (traditional method)
- **Tire Model 2:** SIM measured tire loading/stress – Uniformly distributed vertical loading (20 kN) and average vertical contact stress of 613 kPa, assumed to be of circular shape (i.e., disk) with restriction on the diameter of the disk, i.e., diameter not exceeding the tire width.
- **Tire Model 3:** Representing Tire Model 2 but with four circular disks staggered in two layers (to mimic the measured shape of vertical contact stress in the tire patch.
- **Tire Model 4:** Representing data measured for Tire Model 2 but with multiple (202) smaller circular disks with a radius of 4.85 mm (to mimic the measured shape of vertical contact stress in the tire patch).

The purpose of the various analyses that follow here is to demonstrate the effect of different tire models on pavement responses, as obtained from (1) the vertical stress reaction, and (2) the Strain Energy of Distortion (SED) [26], [33]. The SED discussed in this paper is according to Timoshenko and Goodier [33], and is defined as the quantity of strain energy stored per unit volume of the material that can be used as a basis for determining the limiting stress at which failure occurs. For this, to be applied to isotropic materials, it is important to separate this energy into two parts; one due to the change in volume and the other due to the distortion, and consider only the second part in determining the strength. Whatever the stress system, failure occurs when the strain energy of distortion reaches a certain limit. Now, total strain energy per unit volume, V_0, can be expressed by using Hooke's law as follows:

$$V_0 = \frac{1}{2E}\left(\sigma_x^2 + \sigma_y^2 + \sigma_z^2\right) - \frac{\nu}{E}\left(\sigma_x\sigma_y + \sigma_y\sigma_z + \sigma_z\sigma_x\right) + \frac{1}{2G}\left(\tau_{xy}^2 + \tau_{yz}^2 + \tau_{xz}^2\right) \quad \text{.....(1)}$$

where: σ_i and τ_{ij} are normal stress in the i-direction and shear stress on the i-face along the j-direction, respectively. See also [21].

Whereas the component of strain energy due to distortion (*SED)*, can then be expressed as follows:

$$SED = V_0 - \frac{1-2\nu}{6E}\left(\sigma_x + \sigma_y + \sigma_z\right)^2 \quad \text{.....(2)}$$

It is the notion in this paper that with this approach, points within the pavement structural system that have higher values of strain energy of distortion (SED) (so-called "*hot-spots*") will potentially fail first before points with relatively lower values, as was also indicated by Perdomo and Nokes [24] and De Beer *et al* [6]. Ideally, this should be linked with the formation of traffic associated crack formation and potholes, and needs further research to quantify, possible by way of appropriate empirical transfer functions.

Software dubbed “TyreStress” was developed to interpolate and also export the SIM measured contact load/stress in the format of the above different tire models for the purpose of pavement analyses (TyreStress is the so-called “delivery system” for tire contact stress/load for pavement design). The mechanistic-empirical pavement analyses were done using general (optimized) multilayer linear elastic methodology with the possibility of multiple circular 3D tire loadings [19], [20], [21]. An example of the selection screen of TyreStress software is shown in FIG. 24.

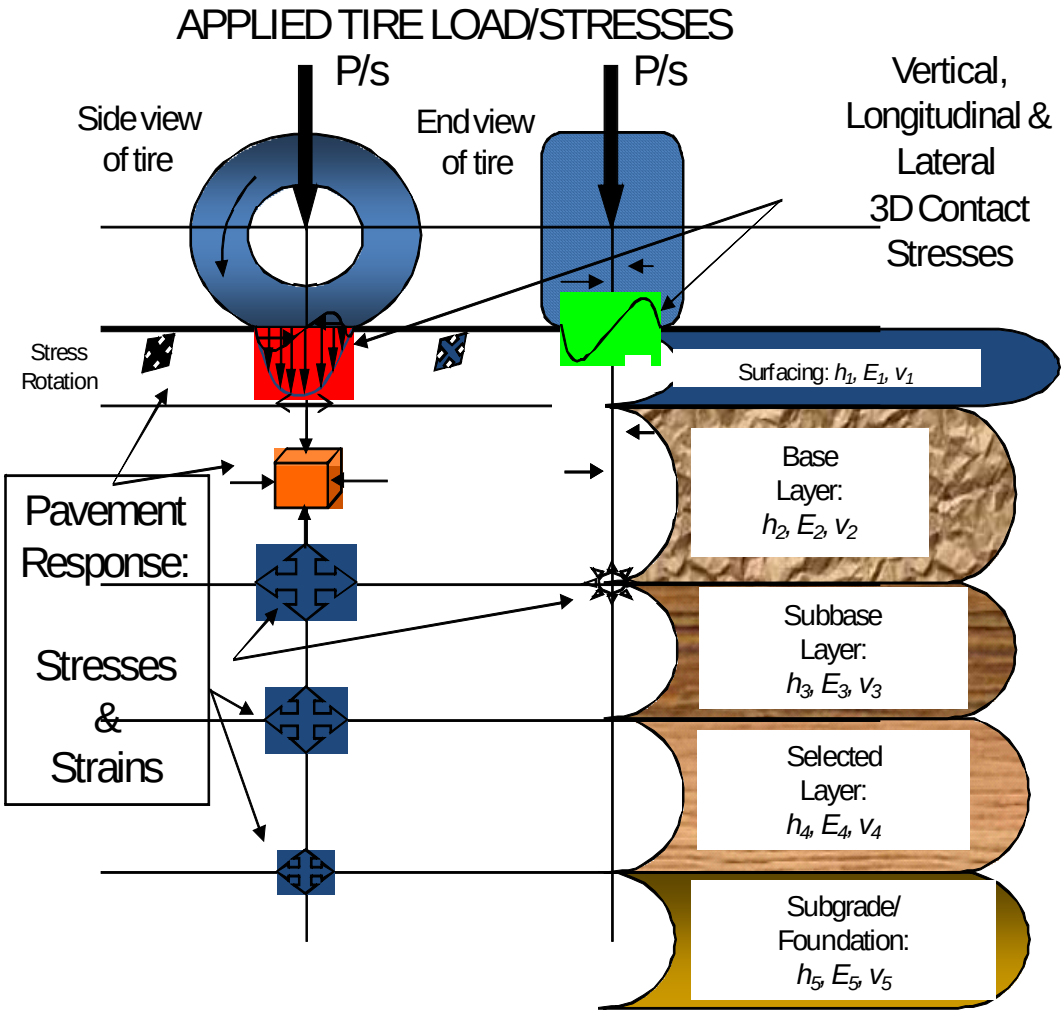

FIG. 23. Typical schematic of a multilayer road pavement structural design problem with (real) tire loading. [Note: h_i = layer thickness; E_i = elastic modulus; v_i = Poisson's Ratio – for layer i, where i = 1,2,3…, and P = tire load, σ = stress]

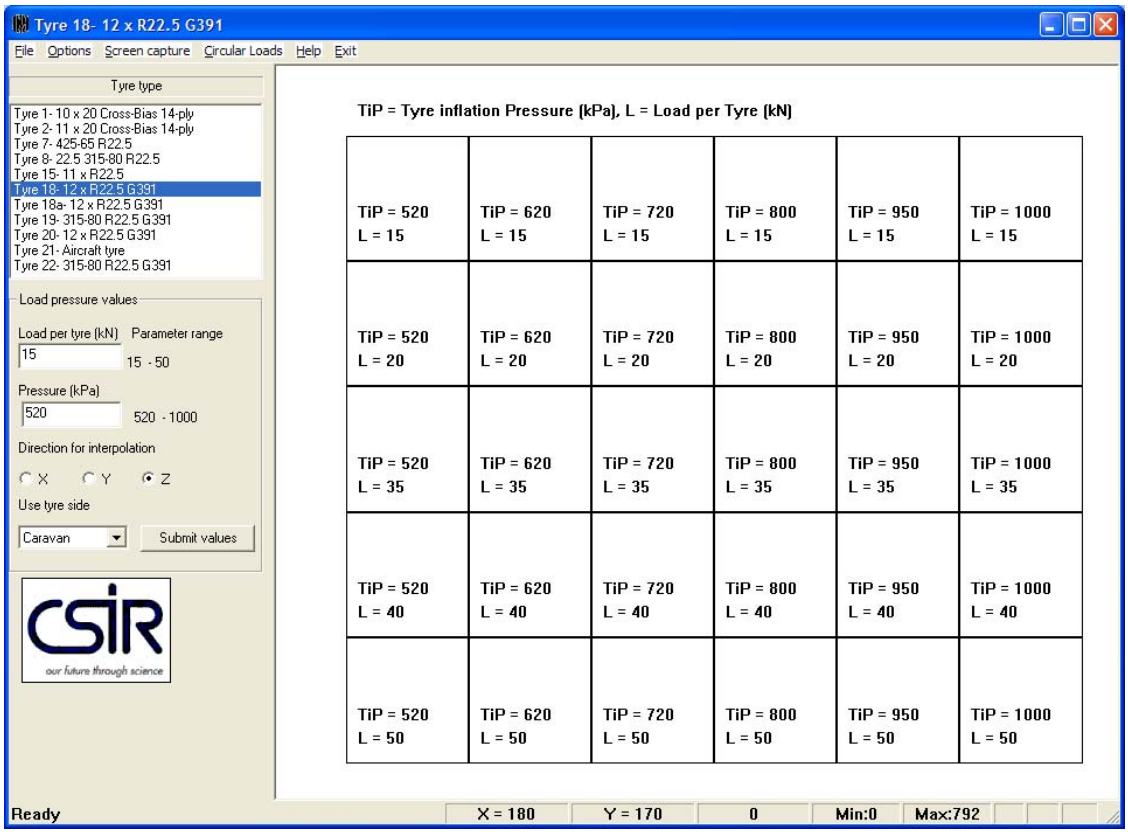

FIG. 24. Example of the TyreStress tire selection screen, where TiP = Tire Inflation Pressure in kPa and L = Tire Loading in kN of the test. [Several tire types are available in the TyreStress database towards the top left of this screen.]

For the case investigated in this paper, i.e., "Tire 18: 12 R22.5" at load of 20 kN and inflation pressure of 520 kPa, an image of the measured vertical contact stress (Z) footprint is shown at the bottom right of FIG. 25. An average vertical contact stress of 613 kPa (over the contact patch of 326 cm^2) is estimated from the measured data for this tire at 20 kN load and 520 kPa inflation pressure. The radius of the equivalent circular area is given as 102 mm. The maximum contact stress within the footprint area in this case is given as 792 kPa. It should be noted that the images in FIG. 25 to FIG. 28 are constructed from data obtained by pentic-order polynomial fitting and topological

interpolation from measured tire data (see various examples of *measured* data given in FIG. 14, FIG. 15, FIG. 16, FIG. 17, FIG. 18 FIG. 19 and FIG. 21), similar to what was reported by Fernando *et al.* in 2006 [15], but for South African tire data. (For completeness of the polynomial fitting and associated topological interpolation scheme applied on the measured tire data, as referenced TyreStress software in [4], see Appendix A for a summary). Further, cross-sections of the *interpolated* contact stress data are shown above and towards the left of the footprint images in FIG. 25 to FIG. 28. The stress values are in kPa units. A further functionality of TyreStress software is to enable the exporting of tire contact stress (or load) data in idealized format or as raw *interpolated* data. 0, FIG. 27 and FIG. 28 illustrate Tire Models 2, 3 and 4 respectively, for which the data were exported for the pavement analyses used in this study.

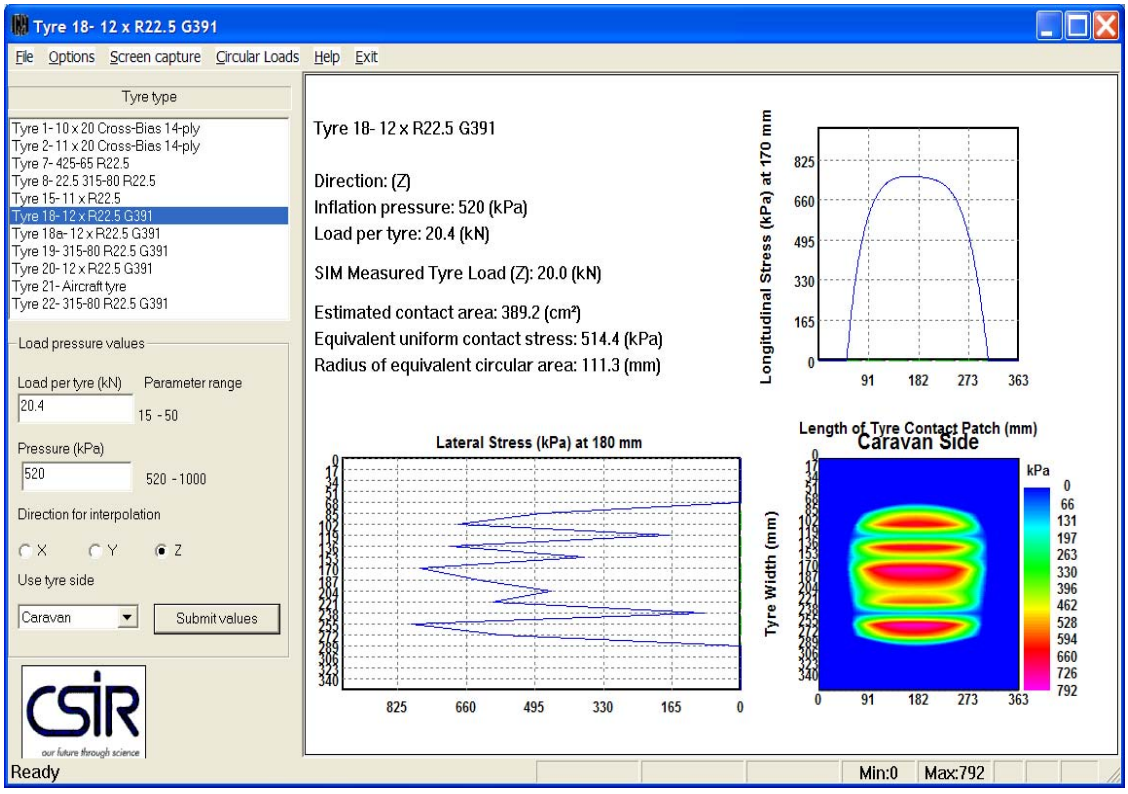

FIG. 25. Representation of *interpolated* tire data for "Tire 18: 12R22.5", at 20 kN and 520 kPa tire inflation pressure. An average vertical contact stress of approximately 520 kPa (over the contact patch of 390 cm^2) is shown.

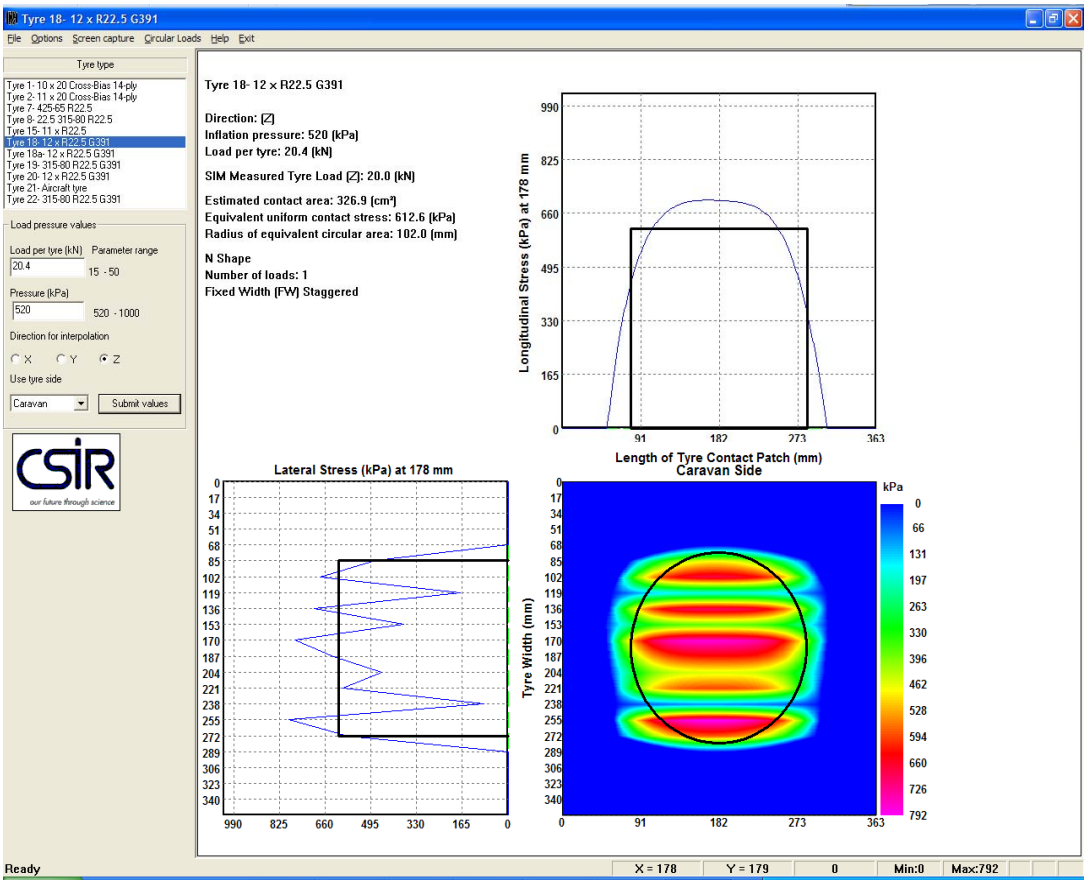

FIG. 26. Representation of Tire Model 2: SIM measured tire loading/stress – Uniformly distributed vertical loading (20 kN) and average vertical contact stress of 613 kPa, assumed to be of circular shape (i.e., disk) with restriction on the diameter of the disk, i.e., diameter not exceeding the tire width, i.e., “fixed width” (FW).

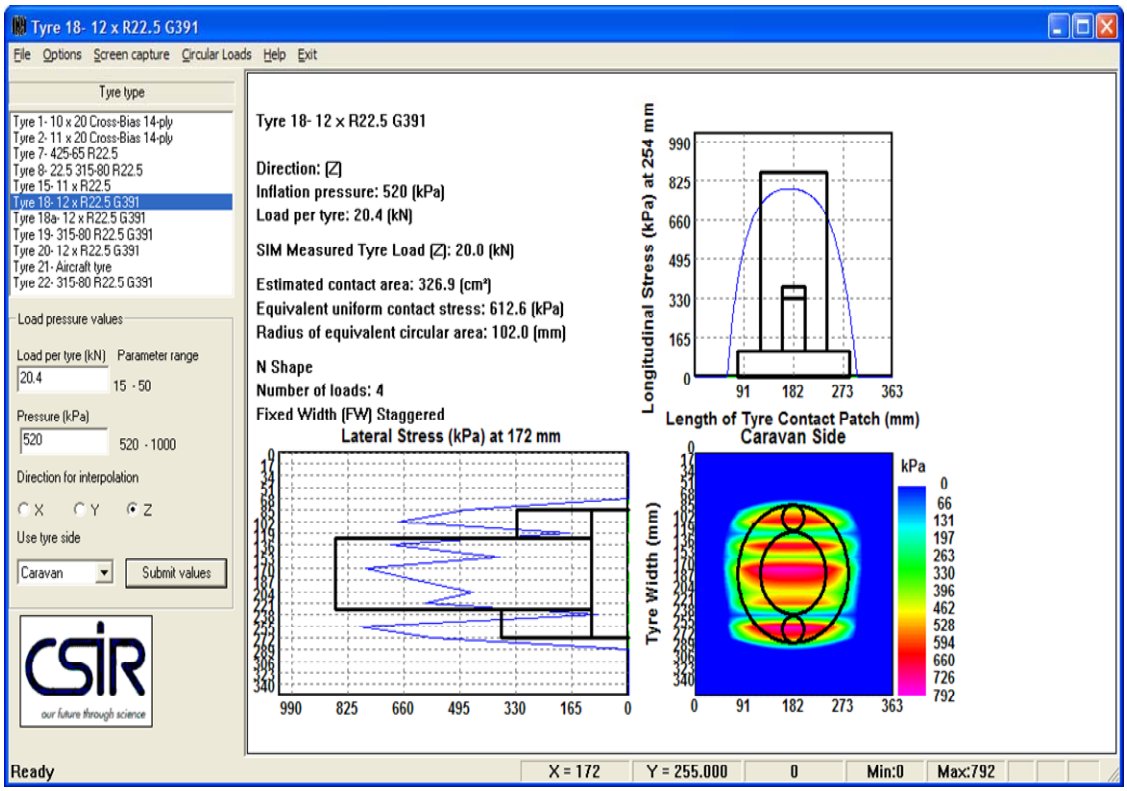

FIG. 27. Representation of Tire Model 3: Representing Tire Model 2 but with four circular disks staggered in two layers (to mimic the measured shape of vertical contact stress in the tire patch).

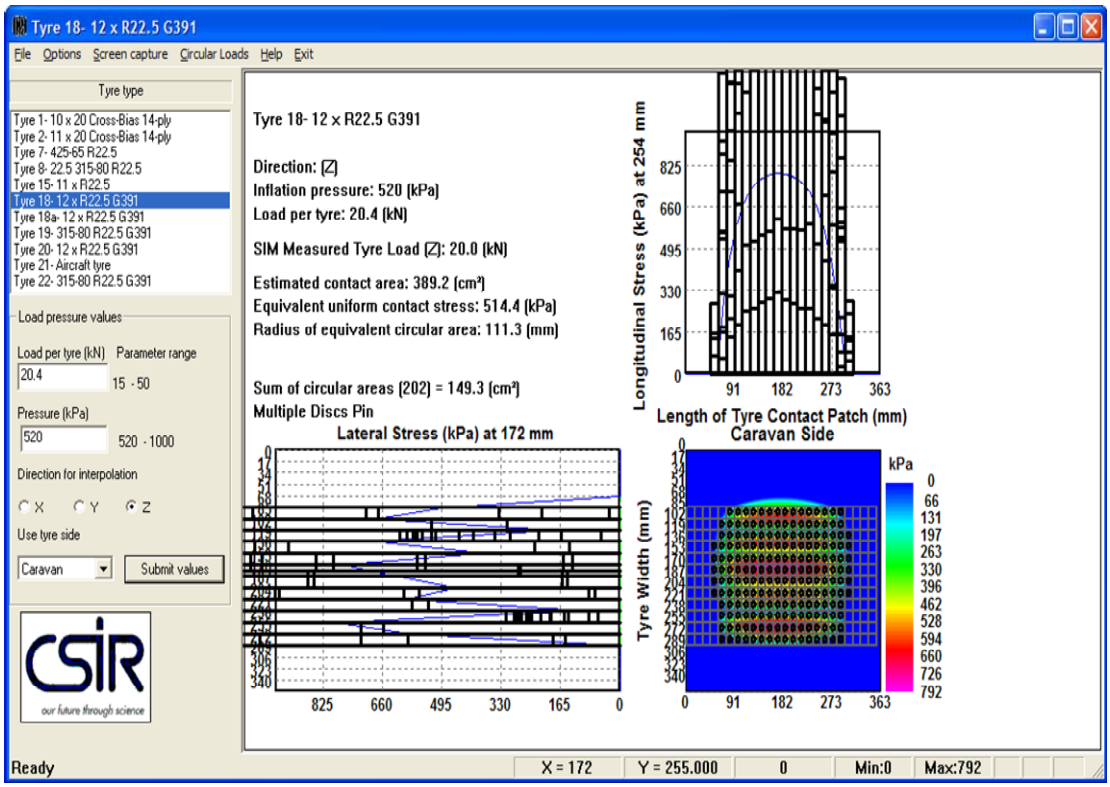

FIG. 28. Representation of Tire Model 4: Representing data measured for Tire Model 2 but with multiple (202) smaller circular disks (to mimic the measured shape of vertical contact stress in the tire patch).

The definition of the 5-layer flexible road pavement investigated in this study is given in FIG. 29. The pavement analyses were done with multilayer linear elastic methodology using the basic *me*PADS software [32] available in South Africa.

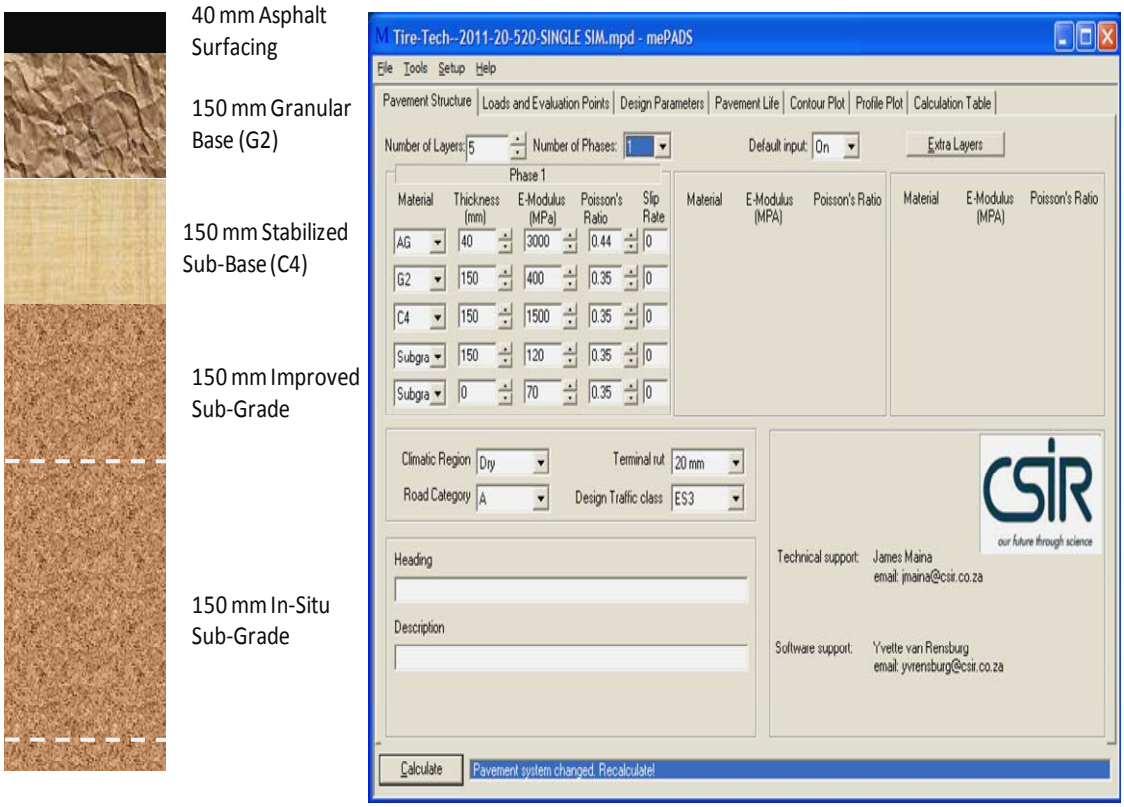

FIG. 29. Definition of the five-layer road pavement structure used for the various analyses. Materials according to [3] and screen clip from *me*PADS software [32].

The images of the four tire models discussed above are also summarized in FIG. 30, FIG. 31, FIG. 32 and FIG. 33, respectively. The vertical stress distribution through the pavement depth under the four tire models is illustrated in FIG. 34, FIG. 35, FIG. 36 and FIG. 37. The maximum vertical stress (Normal Stress ZZ) was found to be on the surface of the pavement, in the center area of the tire patch. The computed vertical stresses ranged from 520 kPa to 2,490 kPa for the four tire models. Note the rather irregular pattern of vertical stress in FIG. 37 for Tire Model 4, compared to the result of other three tire models. The four different Strain Energy of Distortion (SED) distributions through

the pavement are illustrated in FIG. 38, FIG. 39, FIG. 40 and FIG. 41. These figures indicated two nominal peak values of SED through the pavement structure, one on the surface of the 40 mm asphalt layer near the center of the tire patch, and the second at the bottom of the asphalt layer at a depth of 40 mm, also near the center of the tire patch. The maximum SED values at the bottom of the 40 mm asphalt layer ranged between 157 Nm/m^3 and 337 Nm/m^3. The positions of the peak SED values can be interpreted as "hot spots" for potential road layer failure, as was discussed in by De Beer *et al.* in 1997 [7].

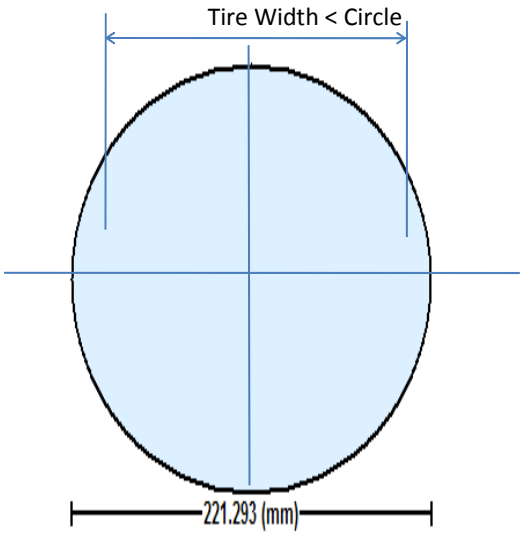

FIG. 30. Tire Model 1(Traditional method – no limit on radius)

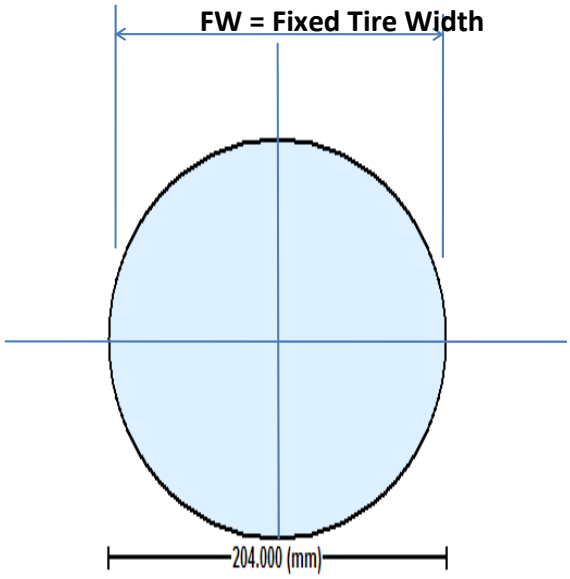

FIG. 31. Tire Model 2 (Radius limited to Fixed Tire Width, FW)

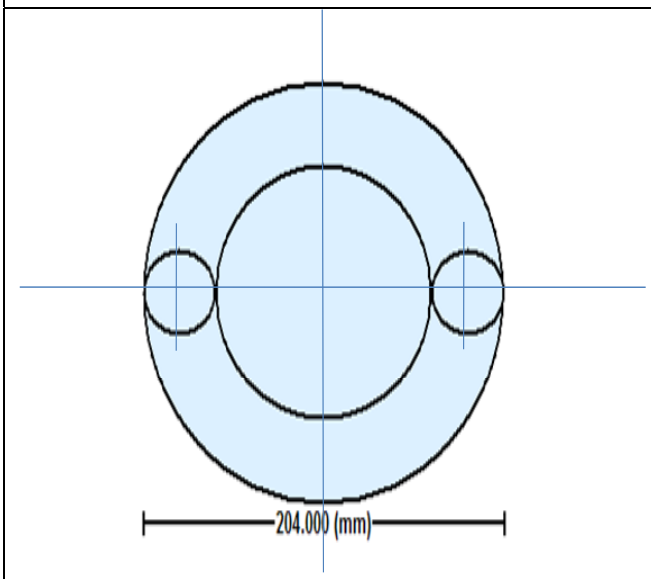

FIG. 32. Tire Model 3 (four disks, staggered, maximum radius limited to FW).

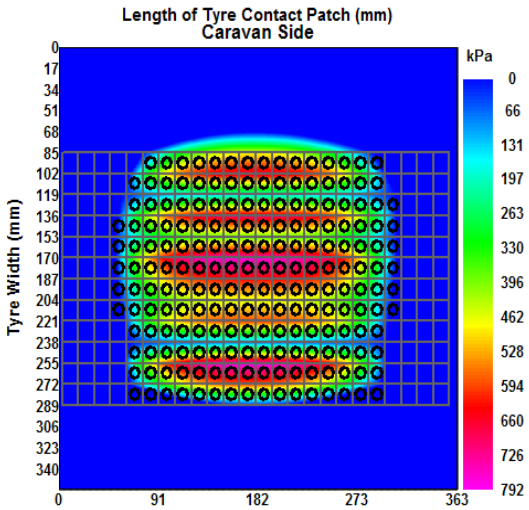

FIG. 33. Tire Model 4 (202 individual circular loads, radius = 4.85 mm).

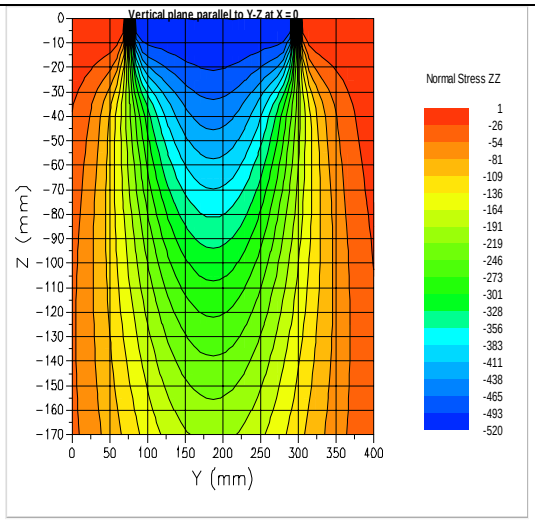

FIG. 34. Vertical stress reaction through pavement (top 170 mm): Tire Model 1 (maximum stress = 520 kPa on surface).

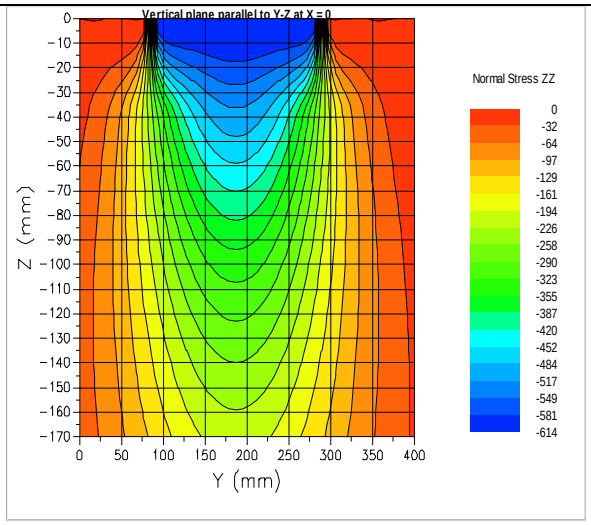

FIG. 35. Vertical stress reaction through pavement (top 170 mm): Tire Model 2 (maximum stress = 614 kPa on surface).

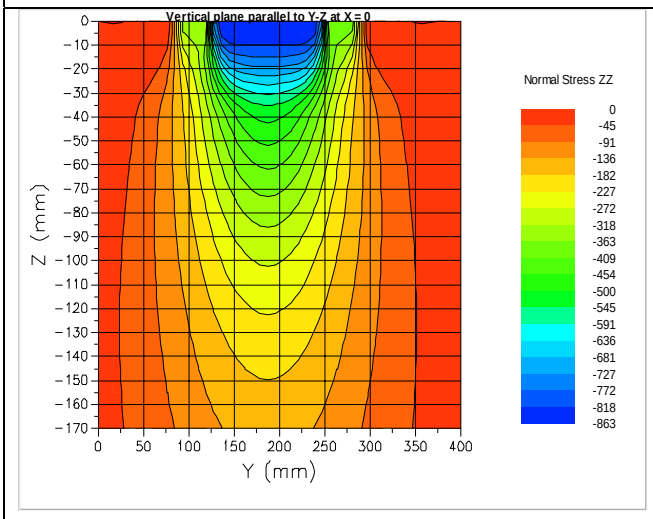

FIG. 36. Vertical stress reaction through pavement (top 170 mm): Tire Model 3 (maximum stress = 863 kPa on surface).

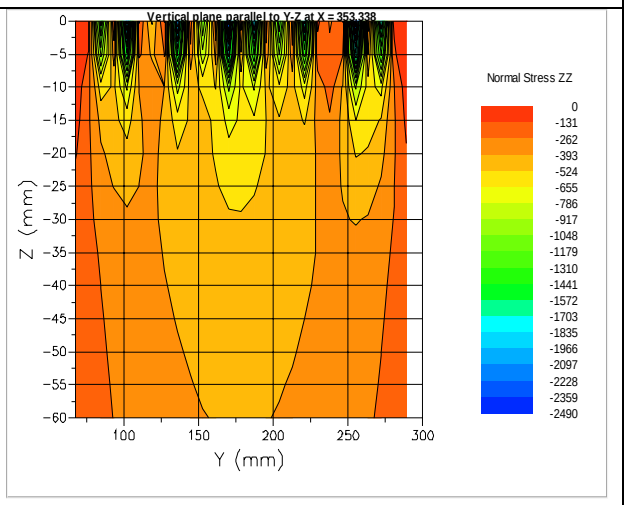

FIG. 37. Vertical stress reaction through pavement (top 170 mm): Tire Model 4 (maximum stress = 2,490 kPa on surface).

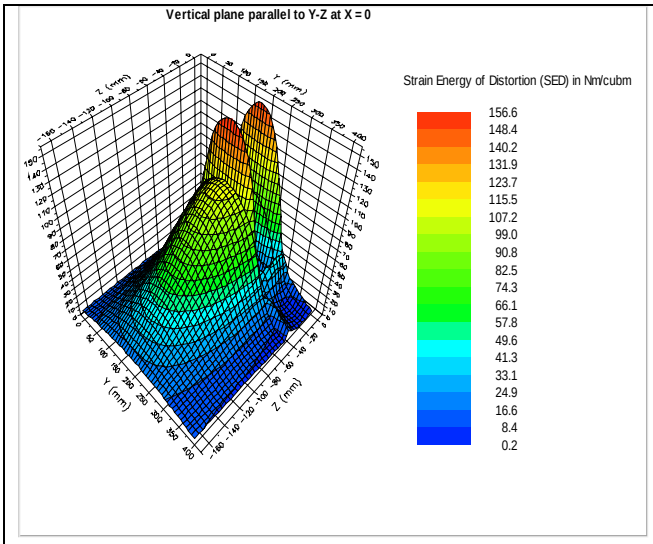

FIG. 38. Strain Energy of Distortion (SED) through pavement (top 170 mm): Tire Model 1 (maximum SED = 157 Nm/m^3 at 40 mm depth).

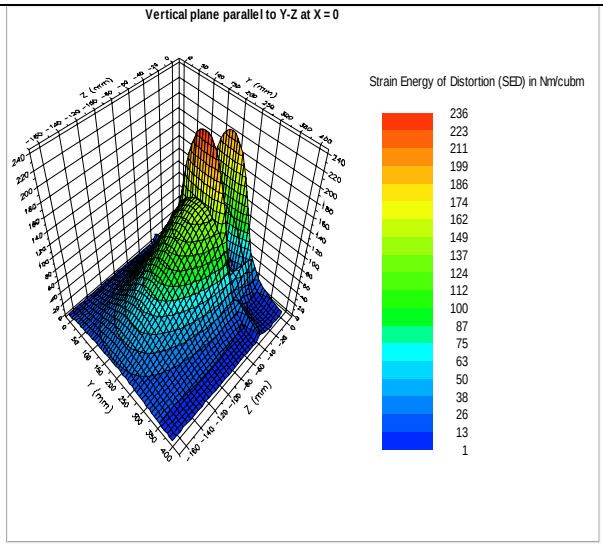

FIG. 39. Strain Energy of Distortion (SED) through pavement (top 170 mm): Tire Model 2 (maximum SED = 236 Nm/m^3 at 40 mm depth).

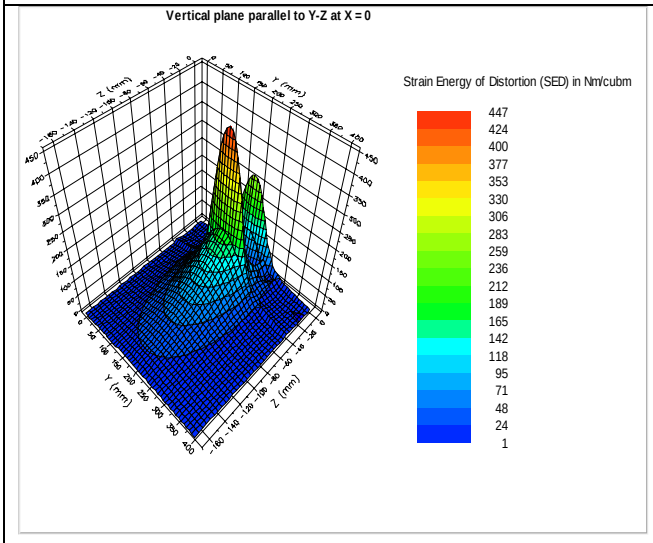

FIG. 40. Strain Energy of Distortion (SED) through pavement (top 170 mm): Tire Model 3 (maximum SED = 337 Nm/m^{3}at 40 mm depth).

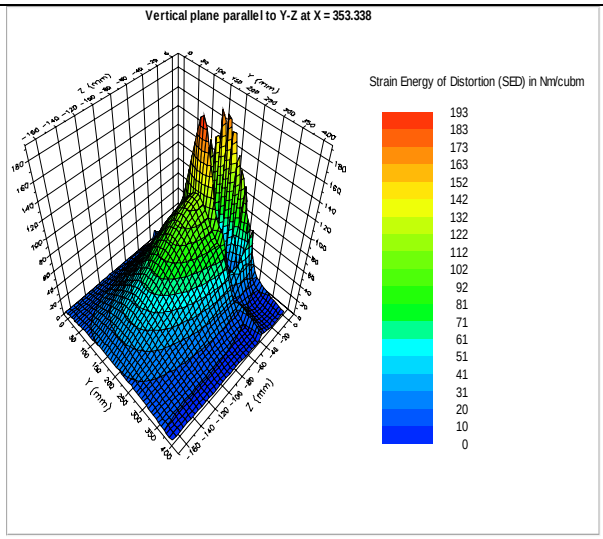

FIG. 41. Strain Energy of Distortion (SED) through pavement (top 170 mm): Tire Model 4 (maximum SED = 193 Nm/m^3 at 40 mm depth).

Discussion of Pavement Response

The two selected pavement response parameters, i.e., vertical stress through the pavement as well as the SED, clearly indicate different maximum peak values, depending on the tire model used. In this case a surface contact stress difference of up to 4.5 times was computed between the standard assumption (Tire Model 1) and the case where the tire was modeled as 202 multiple circular disks (Tire Model 4). Also, a change in SED was obtained, peaking under Tire Model 3, and then reducing again in the case of Tire Model 4. These peak SED values occurred both at zero depth (pavement surface) and at the bottom of the 40 mm thin asphalt surfacing layer, with the maximum always at the bottom of the asphalt surfacing layer. It is interesting to note that it seems that the SED peaks at the bottom of this relatively stiffer asphalt layer (modeled with linear elastic modulus (E_1) of 3,000 kPa and Poisson's Ratio ν_1 = 0.44). These peaks of SED are believed to be indicative of the expected potential failure mechanism in this structure (probably fatigue cracking to be initiated at the bottom of the asphalt layer). This is in addition to potential rutting from the surface, indicated by the peak SED at z = 0 mm in the center of the tire contact patch, under the various tire models (see summary of the pavement response data (i.e., computed vertical stress and SED) shown in FIG. 42 and FIG. 43). An attempt was also made to compute expected pavement "life" (or bearing capacity in terms of standard 80 kN axle repetitions) for the pavement and the various tire models investigated here. For the layer bearing capacities in terms of standard 80 kN axles, existing fatigue and layer damage models available in the South Africa were used [31] for the quantitative analyses. The results from Tire Model 1 were compared with those from Tire Model 2, Tire Model 3 and Tire Model 4 for this purpose (see TABLE 2 and TABLE 3). TABLE 2 indicates that the layer fatigue life (or bearing capacity) of the 40 mm asphalt layer (AG layer) is reduced by approximately 64 percent. The bearing capacity of the unbound granular base (G2 layer) is reduced by approximately 6 percent, and that of the lightly cementitious subbase layer (C4 layer) by 10 percent when the tire model is changed from the traditional assumption (i.e., Tire Model 1) to Tire Model 2 (i.e., with SIM measured tire data and fixed width (FW) limitation). Similarly, the layer

"life" of the asphalt (AG layer) is reduced by approximately 94 percent, and that of the unbound base (G2 layer) by approximately 6 percent when the results of Tire Model 1 are compared with those found with Tire Model 3 (see results in TABLE 2). Interestingly, according to Theyse *et al.* [31], the "life" or bearing capacity of the lightly cementitious subbase layer (C4 layer) with regard to both fatigue and crushing failure associated with these layers improved by approximately 70 percent owing to a slightly *reduced* vertical stress on the top of this cementitious subbase (C4 layer). (See TABLE 2 and FIG. 42 at a depth of 190 mm. TABLE 3 summarizes the effect on layer "life" on the same pavement, comparing Tire Model 1 with two positions under Tire Model 4 (total of 202 circular disks of 4.85 mm radius). The two positions (Position 1: X = 353.3376 mm, Y = 255 mm, and Position 2: X = 353.3376 mm, Y = 175 mm, within Tire Model 4 contact patch – see FIG. 42, FIG. 43 and TABLE 2) were selected to demonstrate that different pavement layer "lives" are obtained under a *single* tire contact patch. The specific data from TABLE 3 show that at Position 1 the asphalt layer (AG layer) life increased by 170 percent relative to Tire Model 1, and that of the lightly cementitious layer (C4 layer) by 60 percent. On the other hand, at Position 2 a reduction of 61 percent was computed for the asphalt layer. Relatively minor effects were obtained for the other layers in this pavement. The layer "life" discussed above is in accordance with layer damage laws for mechanistic-empirical pavement analyses discussed in [31].

The above results are interpreted (as with the computed vertical stress) to be dictated by the geometry and characteristics (i.e., tire contact stress patch and its contact shape) of the tire model used for pavement modeling. The importance, therefore, of using a suitable (and hopefully a more rational) tire model for pavement design cannot be overemphasized. More research and analyses are, however, needed to validate the theoretical behavior discussed here, and the results should be updated on the basis of future appropriate research on a wider range of tires and road pavement types.

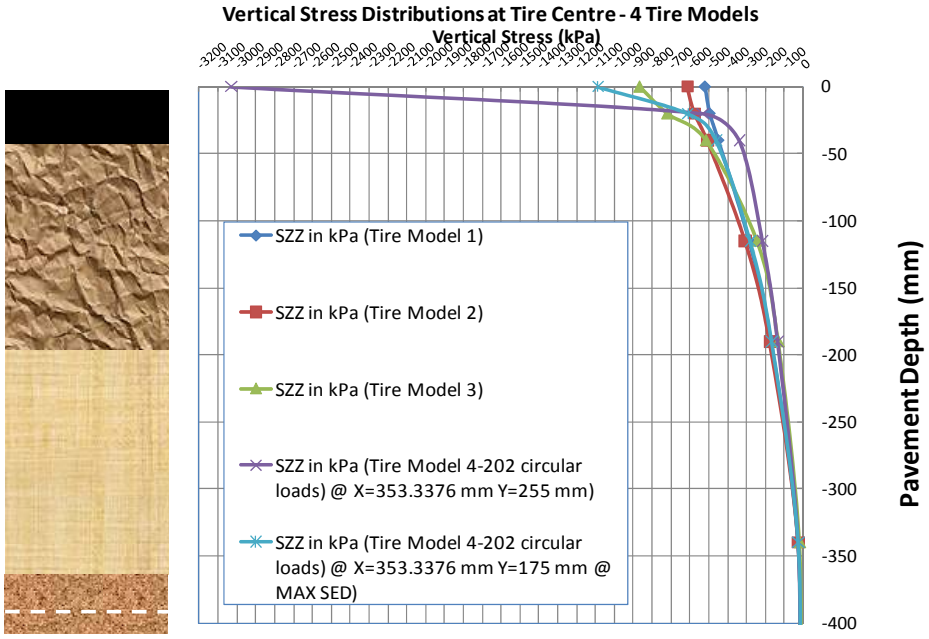

FIG. 42. Summary of the computed vertical stress (Normal Stress ZZ) through pavement depth (this study) for the four tire models used in this paper.

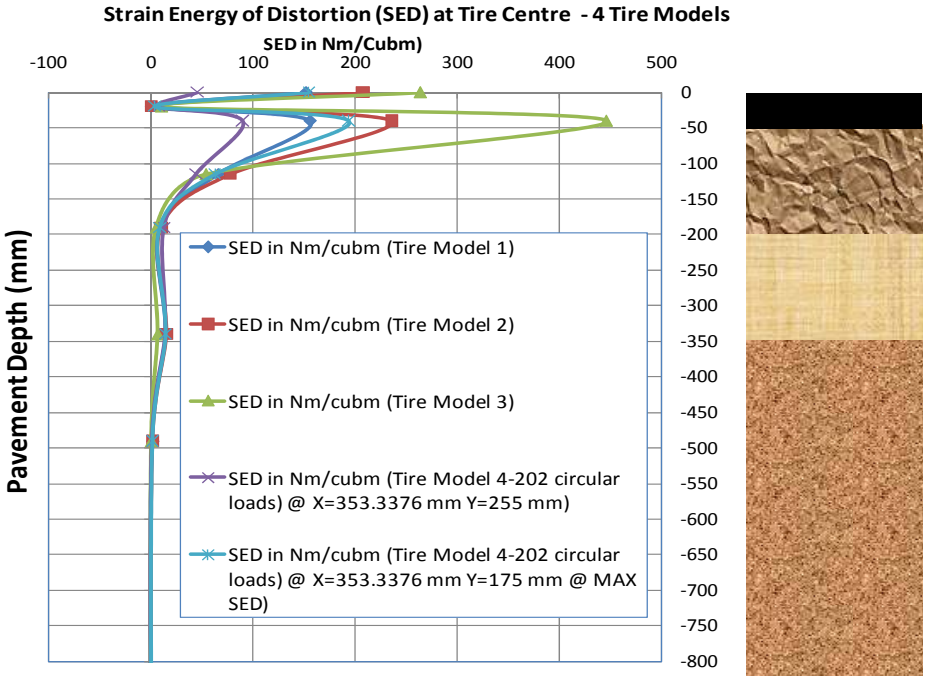

FIG. 43. Summary of the computed SED through pavement depth for the four tire models used in this paper.

TABLE 2. Summary data of layer bearing capacities in standard 80 kN axle loadings and associated changes (in percent) as a result of a different tire model being used. Tire Model 1 compared with results from Tire Model 2 and Tire Model 3.

TIRE MODEL 1: STANDARD - SINGLE 20/520	**Layer bearing capacities**		**Crushing in cemented layers**		**Change (%) as a result of Tire Model 2 relative to Tire Model 1**
Layer	**Life**	**Cemented life**	**Crushing initiation**	**Advanced crushing**	
AG	9.27E+06				-63.86%
G2	2.61E+07				-5.71%
C4	4.35E+06	4.35E+06	4.41E+06	1.51E+07	-1.40%
SUBG 1	2.03E+07				-0.64%
SUBG 2	2.61E+07				-0.44%
TIRE MODEL 2: SIM - SINGLE (FW)	**Layer bearing capacities**		**Crushing in cemented layers**		
Layer	**Life**	**Cemented life**	**Crushing initiation**	**Advanced crushing**	
AG	3.35E+06				
G2	2.46E+07				
C4	4.29E+06	4.29E+06	3.95E+06	1.35E+07	-10.32%
SUBG 1	2.01E+07				
SUBG 2	2.60E+07				
TIRE MODEL 1: STANDARD - SINGLE 20/520	**Layer bearing capacities**		**Crushing in cemented layers**		**Change (%) as a result of Tire Model 3 relative to Tire Model 1**
Layer	**Life**	**Cemented life**	**Crushing initiation**	**Advanced crushing**	
AG	9.27E+06				-94.16%
G2	2.61E+07				-5.92%
C4	4.35E+06	4.35E+06	4.41E+06	1.51E+07	28.81%
SUBG 1	2.03E+07				97.86%
SUBG 2	2.61E+07				99.21%
TIRE MODEL 3: SIM-4 x DISKS-SIM	**Layer bearing capacities**		**Crushing in cemented layers**		
Layer	**Life**	**Cemented life**	**Crushing initiation**	**Advance. crushing**	
AG	5.41E+05				
G2	2.46E+07				
C4	5.61E+06	5.61E+06	7.53E+06	2.58E+07	70.84%
SUBG 1	4.01E+07				
SUBG 2	5.20E+07				

TABLE 3. Summary data of layer bearing capacities in standard 80 kN axle loadings and associated changes (in percent) as a result of a different tire model being used. Tire Model 1 compared with results from Tire Model 4 (both Positions 1 and 2 within tire patch)

TIRE MODEL 1: STANDARD - SINGLE 20/520	**Layer bearing capacities**		**Crushing in cemented layers**		**Change (%) as a result of Tire Model 4 (Position 1) relative to Tire Model 1**
Layer	**Life**	**Cemented life**	**Crushing initiation**	**Advanced crushing**	
AG	9.27E+06				170.43%
G2	2.61E+07				5.44%
C4	4.35E+06	4.35E+06	4.41E+06	1.51E+07	4.36%
SUBG 1	2.03E+07				2.73%
SUBG 2	2.61E+07				1.57%
TIRE MODEL 4: SIM-ALL PINS (202) - Position 1*	**Layer bearing capacities**		**Crushing in cemented layers**		
Layer	**Life**	**Cemented life**	**Crushing initiation**	**Advanced crushing**	
AG	2.51E+07				
G2	2.76E+07				
C4	4.54E+06	4.54E+06	7.07E+06	2.42E+07	60.51%
SUBG 1	2.08E+07				
SUBG 2	2.65E+07				
TIRE MODEL 1: STANDARD - SINGLE 20/520	**Layer bearing capacities**		**Crushing in cemented layers**		**Change (%) as a result of Tire Model 4 (Position 2) relative to Tire Model 1**
Layer	**Life**	**Cemented life**	**Crushing initiation**	**Advanced crushing**	
AG	9.27E+06				-60.78%
G2	2.61E+07				0.59%
C4	4.35E+06	4.35E+06	4.41E+06	1.51E+07	0.48%
SUBG 1	2.03E+07				0.14%
SUBG 2	2.61E+07				0.02%
TIRE MODEL 4: SIM-ALL PINS (202) - Position 2*	**Layer bearing capacities**		**Crushing in cemented layers**		
Layer	**Life**	**Cemented life**	**Crushing initiation**	**Advanced crushing**	
AG	3.63E+06				
G2	2.63E+07				
C4	4.37E+06	4.37E+06	4.62E+06	1.58E+07	4.76%
SUBG 1	2.03E+07				
SUBG 2	2.61E+07				
*** Position 1**	X=353.3376 mm	Y=255 mm			
*** Position 2**	X=353.3376 mm	Y=175 mm			

Key:

AG = Asphalt surfacing layer, 40 mm thick

G2 = Unbound Granular Layer, 150 mm thick

C4 = Lightly Cemented Layer, 150 mm thick

SUBG 1 = Upper Unbound Subgrade layer
SUBG 2 = Lower Unbound Subgrade layer
Cemented life = Life of cementitious layer (C4 layer) [31]
Crushing initiation = Initiation of crushing failure mode of C4 layer [31]
Advanced crushing = Advanced crushing failure mode of C4 layer [31]
Life = Standard 80 kN axle loadings.

Conclusions and Recommendations

It is concluded that:

- Tire-pavement contact stresses can be quantified in 3D, using Stress-In-Motion (SIM) technology.
- "Tire rolling resistance" could potentially be defined by the Static Rolling Resistance force (SRRf) and associated rolling resistance coefficients obtained from the SIM type of testing.
- The tire contact stress/loading results are considered acceptable for advanced mechanistic pavement analysis.
- Current data show that 3D tire pavement contact stresses are complex, and may assist with advanced structural road pavement analysis.
- More sophisticated tire models appear to result in a more realistic road pavement response.
- Current analyses show that "road surfacing layer fatigue life" is reduced by as much as ~ 94 percent by changing the tire model used for mechanistic road pavement design.
- Tire models idealized by several multiple circular loadings could result in different pavement layer "lives" being computed within a single tire contact patch.

It is therefore postulated that “The better the representation of the “real/actual tire-contact stress” regime, the better the road response and hence the design of road pavements – especially near the road surface”. It is believed that an improved understanding of the surface pavement failure mechanisms illustrated in this paper will be possible with the incorporation of improved understanding and quantification of the tire-road interaction mechanisms at the near road surface.

It is recommended that 3D tire road pavement contact stresses be quantified on a wider range of tires, and their effect be incorporated into modern-day road pavement analyses. Ideally, 3D tire pavement contact stresses should be used for the mechanistic-empirical design of road pavement structures, as measured, with minimal idealization of shape and magnitude.

Acknowledgements

The Executive Director of CSIR Built Environment is thanked for permission to publish this paper.

References

[1] Bonse, R. P. H., Kuhn, S. H., Dynamic forces exerted by Moving Vehicles on a Road Surface. Highway Research Board Bulletin, No. 233: Flexible Pavement Design, 1959, pp. 9–32.

[2] Committee of State Road Authorities (CSRA), Structural Design of Flexible Pavements for Interurban and Rural Roads. Technical Recommendations for Highways No. 4 (Draft TRH 4), 1996. ISBN 1-86844-218-7.

[3] Committee of State Road Authorities (CSRA), Guidelines for Road Construction Materials. Technical Recommendations for Highways No. 14 (Draft TRH 14). 1985, 1996. ISBN 0-7988-3311-4.

[4] De Beer M., Fisher C., Van Rensburg Y., Greben J., Maina J. W., Framework for Tyre Contact Stress Information System (T-CSIS): Project A-1. Report: SANRAL/SAPDM/A-1/2010-003, Revision of the South African Pavement Design Method. Project Focus Area: Traffic Demand Analysis, Version: 3rd Draft Report (Unpublished), March 2011.

[5] De Beer, M., Measurement of tyre/pavement interface stresses under moving wheel loads. Proceedings of the Vehicle-Road and Vehicle-Bridge Interaction Conference, June 5–10, 1994, Noordwijkerhout, The Netherlands (DPVT 224), or Heavy Vehicles Systems, Special Series, Int. J. Vehicle Design, Vol. 3, Nos 1–4, 1996, pp. 97–115. ISSN 01433369.

[6] De Beer M, and Fisher C., Contact Stresses of pneumatic tires measured with the Vehicle-Road Surface Pressure Transducer Array (VRSPTA) system for the University of California at Berkeley (UCB) and the Nevada Automotive Test Center (NATC). Confidential Contract Research Report CR-97/053, Volume 1 and Volume 2, June 1997.

[7] De Beer, M., Fisher, C., Jooste, F. J., Determination of pneumatic tyre/pavement interface contact stresses under moving loads and some effects on pavements with thin asphalt surfacing layers. Proceedings of the 8th International Conference on Asphalt Pavements (ICAP '97), Seattle, Washington, August 10–14, 1997.

[8] De Beer M., Kannemeyer, L., Fisher, C., Towards improved mechanistic design of thin asphalt layer surfacings based on actual tyre/pavement contact Stress-In-Motion (SIM) data in South Africa. Proceedings of the 7th Conference on Asphalt Pavements for Southern Africa (CAPSA '99), Theme 5: Innovation in Asphalt Design, Victoria Falls, Zimbabwe, August 29 to September 2, 1999. ISBN 1874968268 (CD).

[9] De Beer, M., Fisher, C., Jooste, F. J., Evaluation of non-uniform tyre contact stresses on thin asphalt pavements, Proceedings of the 9th International Conference on Asphalt Pavements (ICAP 2002), Copenhagen,

2002. (Proceedings available on CD from conference organizers: The Danish Road Directorate, Ministry of Transport, Denmark, and the International Society of Asphalt Pavements (ISAP).

[10] De Beer, M., Fisher. C., Kannemeyer, L., Tyre-pavement interface contact stresses on flexible pavements - quo vadis? Proceedings of the 8th Conference on Asphalt Pavements for Southern Africa (Roads – The Arteries of Africa), Sun City, North West Province, South Africa, 2004.

[11] De Beer, M., Fisher, C., Kannemeyer, L., Towards the application of Stress-In-Motion (SIM). Results in pavement design and infrastructure protection, Proceedings of the 8th International Symposium on Heavy Vehicles, Weights and Dimensions (Loads, Roads and the Information Highway), Misty Hills Conference Center, Muldersdrift, Gauteng, South Africa, 2004.

[12] De Beer, M., Reconsideration of tyre-pavement input parameters for the structural design of flexible pavements, Proceedings of the 10th International Conference on Asphalt Pavements (10th ICAP), Quebec City, Canada, 2006. ISBN: 978-2-550-49009-8 (CD); ISBN: 978-2-550-49008-1 (Printed).

[13] De Beer, M., Stress-In-Motion (SIM) – A new tool for road infrastructure protection? Proceedings of the International Conference on Heavy Vehicles (HV Paris 2008 – ICWIM5), WIM Session 7, May 19–22, 2008, Paris/Marne-la-Vallée, France.

[14] El-Gindy, M., Lewis, H., Development of a Tire/Pavement Contact-Stress Model Based on Artificial Neural Networks. Publication No. FHWA-RD-99-041, January, FHWA, Research, Development, and Technology, Turner-Fairbank Highway Research Center, McLean, VA, USA, 2001.

[15] Fernando, E. G., Musani, D., Park, D-W., Liu, W., Evaluation of effects of tire size and inflation pressure on tire contact stresses and pavement response, Report FHWA/TX-06/0-4361-1, August, Texas Transportation

Institute, The Texas A&M University System, College Station, Texas, USA, 2006. See Pavement Responses to Loading Last visited on June 18, 2010 – URL: http://tti.tamu.edu/documents/0-4361-1.pdf. Date assessed March 19, 2012.

[16] Freeme, C. R., De Beer, M., Viljoen, A. W., The behaviour and mechanistic design of asphalt pavements. Proceedings of the 6th International Conference on Structural Design of Asphalt Pavements, July 13–17, 1987, Ann Arbor, Michigan, USA, pp. 333–343.

[17] Gillespie, T. D., *Fundamentals of Vehicle Dynamics.* Society of Automotive Engineers, Inc., Warrendale, PA, USA, 1992.

[18] Huang, Y. H., *Pavement Analysis and Design,* Prentice-Hall International, Englewood Cliffs, NJ, USA, 1993. ISBN 0-13-655275-7.

[19] Maina, J. W., Matsui, K., Developing software for elastic analysis of pavement structure responses to vertical and horizontal surface loadings, Transportation Research Record, No. 1896, 2004, pp. 107–118.

[20] Maina, J. W., Denneman, E., De Beer, M., Introduction of new road pavement response modelling software by means of benchmarking, Proceedings of the 27th Annual Southern African Transport Conference, South Africa, July 7–11, 2008. ISBN: 978-1-920017-34-7.

[21] Maina, J. W., De Beer, M., Improved performance evaluation of road pavements by using measured tyre loading. Proceedings of the 2nd CSIR Biennial Conference (Science Real and Relevant), November 17–18, 2008, CSIR International Convention Centre, Pretoria, South Africa, p 13. ISBN: 978-1-920017-34-7.

[22] Myers, L. A., Roque, R., Ruth, B. E., Drakos, C., Measurement of contact stresses for different truck tire types to evaluate their influence on near-surface cracking and rutting, Transportation Research Record, No. 1655, 1999, pp 175–184.

[23] Myers, L. A., Roque, R., Birgisson, B., Propagation mechanisms for surface-induced longitudinal wheel path cracks. Transportation Research Record, No. 1778, 2001, pp 113–122.

[24] Novak, M., Birgisson, B., Roque, R., Three-dimensional finite element analysis of measured tire contact stresses and their effects on instability rutting of asphalt mixture pavements, Proceedings of the 82nd Transportation Research Board Annual Meeting, Washington D.C., MD, USA, January 12–16, 2003.

[25] Ooura,T. and Mori, M. "The Double Exponential Formula for Oscillatory Functions over Half Infinity Integral", Journal of Computational and Applied Mathematics 38, 1991, pp.353-360.

[26] Perdomo, D., Nokes, B., Theoretical analysis of the effects of wide-base tires on flexible pavements. In: Rigid and Flexible Pavement Design and Rehabilitation (Pavement Design, Management, and Performance), Transportation Research Record, No. 1388, 1993, pp. 60–69.

[27] Priest A. L., Timm, D. H., Mechanistic comparison of wide-base single versus standard dual tire configurations. In: Pavement Rehabilitation, Strength and Deformation Characteristics, and Surface Properties-Vehicle Interaction, Transportation Research Record, No. 1949, 2006, pp 155–163.

[28] Roque, R., Myers, L. A., Ruth, B. E., Loading characteristics of modern truck tires and their effects on surface cracking of asphalt pavements, Proceedings of the 5th International Conference on the Bearing Capacity of Roads and Airfields (BCRA '98), July 6–8, Trondheim, Norway, Vol. 1, 1998, pp. 93–102.

[29] Roque R., Myers, L. A., Birgisson, B., Evaluation of measured tire contact stress for the prediction of pavement response and performance. Transportation Research Record, No. 1716, 2000, pp 73–81.

[30] Soon, S., Drescher, A., Stolarsky, H. K., Tire-induced surface stresses in flexible pavements. Proceedings of the 82nd Transportation Research Board Annual Meeting, Washington DC, MD, USA, January 12–16, 2003.

[31] Theyse, H. L., De Beer, M., Rust, F. C., Overview of the South African Mechanistic Pavement Design Analysis Method. Proceedings of the 75th Annual Transportation Research Board Meeting, January 7–11, Washington, D.C., MD, USA, TRR 1539, 1996, pp. 6–17. ISBN 0309059127.

[32] Theyse, H. L., Muthen, M., Pavement Analysis And Design Software (Pads) based on the South African Mechanistic-Empirical Design Method, Proceedings of the 19th Annual South African Transport Conference (SATC 2000), July, 2000, Pretoria, South Africa.

[33] Timoshenko, S., Goodier, J. N. *Theory of Elasticity*, 2nd Ed., New York, McGraw-Hill, Inc., 1951.

[34] Van Vuuren, D. J., Tyre pressure and its effects on pavement design and performance. National Institute for Road Research, Council for Scientific and Industrial Research, Report RR 192, Pretoria, South Africa, 1974.

[35] Yoder, E. J., Witczack, K. M. W., *Principles of Pavement Design*, 2nd Ed., New York, Wiley-Interscience, 1975. ISBN 0-471-97780-2.

[36] http://www.csir.co.za/Built_environment/brochures.html. Date assessed March 19, 2012.

APPENDIX A

Polynomial fitting and data interpolation methodology for tire contact stress/force measurements from SIM system

Topological interpolation in the TyreStress program

The TyreStress equipment gives data on the z, x or y – load (or stress if divided by area) for a range of values of the tyre inflation pressure P and applied tyre loading L. Here z refers to the downward pressure (so this load is always positive if z points downward), y refers to the lateral movement (across the width of the tyre), and x refers to the longitudinal load in the direction of the tyre. The measurements are done through an array of instrumented pins (or sensors) that are arranged on a horizontal line in the lateral direction (perpendicular to the direction of the tyre). When the tyre moves, different parts of the tyre touch the array of instrumented pins, or sensors (the lateral position characterized by the variable λ), and the position of the tyre is translated into a longitudinal position via the linear relationship $\xi = t\,v$, where $v = (\vec{v})_x$ is the speed along the positive x-axis. Measurements are done for different values of P and L and each (P, L) pair leads to a different load pattern in a different tyre domain (λ, ξ) where the loads are non-zero. The set of measurements then leads to a grid of measured values. The TyreStress software was developed for ease of tire stress/load data viewing and data exporting.

Since the user of the TyreStress software is generally interested in values other than the measured (P, L) pairs, an interpolation scheme is developed to provide intermediate results. Since the tyre domain (λ, ξ) changes its boundaries from one (P, L) pair to another, the interpolation routine has to recognize these topological properties and therefore interpolation is not straightforward. To accommodate the changing boundaries, a topological interpolation routine is developed which recognizes the boundaries and determines an appropriate set of loads corresponding to a desired (P, L) set. Part of this interpolation procedure involves the definition of filters to decide which small measured values represent noise and which ones are small but real.

The notation is defined first. The measured x, y and z loads are indicated by:

$$\{\xi_i, x_i, i = 1 \cdots N\}, \qquad \{\xi_i, y_i, i = 1 \cdots N\} \quad \text{and} \quad \{\xi_i, z_i, i = 1 \cdots N\} \tag{A1}$$

where the index i runs over the number of measurements per tyre, i.e., over different values of $\xi_i = t_i \, v$. Every pin (indicated by $\lambda \in \{\lambda_i, i = 1 \cdots N_\lambda\}$) has its own record. The surface of the tire is mapped via the variables (ξ, λ). Measurements are made for a range of $P \in \{P_i, i = 1 \cdots N_P\}$, and $L \in \{L_i, i = 1 \cdots N_L\}$ values. The idea is to provide interpolation between these (P_i, L_j) pairs. In the graphs of the TyreStress system the loads are shown in the (ξ, λ) plane, by means of 3D plots. The topology of the tire implies that measurements in the (ξ, λ) plane are correlated as they refer to the same physical object (the surface of the tire). This translates into the demand for continuity of the loads/stresses in terms of these variables.

In practise, it is more important to enforce the continuity in ξ as there are lots of measurements so that the results need to be smoothed to get a continuous representation. There are only 21 pins, so at most there can be 21 significant λ measurements and these can best be treated as discrete cases. If a polynomial is interpolated between too few points, one may get low-frequency oscillations between the points, which is not desirable. Hence, λ is treated as another parameter, which can be included in the (P, L) set. This simplifies the interpolation procedure considerably as one now only has continuity constraints in one variable. The measurements are now fitted as a function of ξ with a polynomial of degree M (it is suggested that $M = 7$ be used). Consider, for example, the z load/stress:

$$\{\xi_i, z_i, i = 1 \cdots N\} \tag{A2}$$

Before one can fit a polynomial one has to identify the area where the values are non-zero, since the inclusion of zeroes in the construction of the polynomial would invalidate the result. One determines the first value of ξ_i where $|z_i|$ is larger than a *cut-off* value ε_z, and is not immediately followed by a value lower than ε_z in the next two measurements. Formally, this prescription can be defined as follows:

$$\left\{ N_{\min} = \min \; j \middle| \, |z_j| > \varepsilon_z, |z_{j+1}| > \varepsilon_z, |z_{j+2}| > \varepsilon_z, j = 1 \cdots N \right\} \tag{A3}$$

$$\left\{ N_{\max} = \max \; j \middle| \, |z_j| > \varepsilon_z, |z_{j-1}| > \varepsilon_z, |z_{j-2}| > \varepsilon_z; j = 1 \cdots N \right\} \tag{A4}$$

with boundaries: $\xi_{\min} = \xi_{N_{\min}}$ and $\xi_{\max} = \xi_{N_{\max}}$. The cut-off ε_z can be chosen to be a weighted means of the measurement error and the maximum measurement value. The set of $N_{\max} - N_{\min} + 1$ pairs is now defined:

$$\{\xi_i, z_i; i = N_{\min} \cdots N_{\max}\} \tag{A5}$$

and fits a polynomial $F(\xi) \approx z$:

$$F(\xi) = a_0 + a_1\xi + \cdots + a_M\xi^M; N_{\max} - N_{\min} + 1 \geq M + 1 \tag{A6}$$

where the degree M must be smaller than the number of non-trivial measurements points -1. Fits of datasets that have fewer than eight significant points if $M = 7$ have to be disallowed. The values of $\xi_{\min}$ and $\xi_{\max}$ can be refined once one has constructed this polynomial by redefining them as the values of ξ where the polynomial passes through zero. Due to the filtering procedure, one normally should have $\xi_{\min} < \xi_{N_{\min}}$ and $\xi_{\max} > \xi_{N_{\max}}$. However, in those cases where a measurement point lies outside of this interval, it should be eliminated from the fitting procedure. The ideal degree of the polynomial is about $M = 7$: low enough for it not to lead to unphysical oscillations (overfitting) and high enough for it to be able to capture sufficient detail in the tire profile. The parameters a_i are fixed by an χ^2 fitting procedure. Since this requires sums over powers of ξ (up to a power of $2M$), it might be wise to renormalize the values to avoid excessively large or small numbers. This problem also forewarns that polynomials of higher degree ($M > 7$) may lead to numerical instabilities in the determination of the parameters a_i.

These polynomials are now interpolated between different sets of triplets (P_i, L_j, λ_k). One problem is that in the lateral direction λ there will also be an upper and lower boundary beyond which the values vanish. In the current representation this will mean that for those values of λ all coefficients a_i will be zero, and $\xi_{\min}$ and $\xi_{\max}$ are thus undetermined. The coefficients a_i between different triplets (P_i, L_j, λ_k) can now be interpolated. This would yield a complete representation of the full polynomial in the ξ direction. However, there are various problems with this method. By interpolating the values of the parameters a_i one does not constrain oneself to the ranges $[\xi_{\min}, \xi_{\max}]$ as the boundaries are imposed externally and are not implicit in the

coefficients a_i. In practise, this means that the new polynomial may exhibit oscillatory behavior near the new boundaries, which is undesirable. The other problem is that the values of a_i depend on where we chose the origin in ξ space. If the choices of origins for two triplets (P_i, L_j, λ_k) do not match perfectly (in some topological sense), then the interpolation of the corresponding a_i does not have the intended natural meaning and the interpolation will not have the desired result.

An inherently more robust procedure is to interpolate the values of the polynomials themselves, in which case the values of the polynomials, rather than their coefficients, form the input to the interpolation. In this case we can also have polynomials M of different degrees for different (P_i, L_j, λ_k) values, and we are less sensitive to the choice of origin along the ξ axis. To find an interpolated value for a definite (P, L, λ) set we interpolate linearly within a cube with eight external corners (P_i, L_j, λ_k). Extrapolations will not be tolerated to avoid unstable results. However, even in this case we have a problem. By interpolating for a desired value ξ, we may go outside the interval $[\xi_{\min}, \xi_{\max}]$ for one or more of the eight triplets. If we set the polynomials equal to zero, we can get cusp behavior near the boundaries. The solution to this problem is to rescale the value of ξ for each triplet separately. This procedure contains two steps. First, the required observable F for the parameter set (ξ, P, L, λ) needs to be written in terms of the eight known polynomials at the external corners:

$$\begin{aligned} F(\xi,P,L,\lambda) &= \frac{\lambda-\lambda_{h+1}}{\lambda_h-\lambda_{h+1}}\frac{P-P_{m+1}}{P_m-P_{m+1}}\frac{L-L_{n+1}}{L_n-L_{n+1}}F(\xi_{mnh}(\xi),P_m,L_n,\lambda_h)+\{n\leftrightarrow n+1\} \\ &+\{m\leftrightarrow m+1\}+\{h\leftrightarrow h+1\}+\{m\leftrightarrow m+1,n\leftrightarrow n+1\}+\{h\leftrightarrow h+1,n\leftrightarrow n+1\} \\ &+\{h\leftrightarrow h+1,m\leftrightarrow m+1\}+\{h\leftrightarrow h+1,m\leftrightarrow m+1,n\leftrightarrow n+1\}, \end{aligned} \tag{A7}$$

where $\xi_{\min}(P,L,\lambda) < \xi < \xi_{\max}(P,L,\lambda)$. $\xi_{\min}(P,L,\lambda)$ and $\xi_{\max}(P,L,\lambda)$ are ordinary interpolations of the eight known pairs $[\xi_{\min}, \xi_{\max}]$:

$$\begin{aligned} \xi_{\max}(P,L,\lambda) &= \frac{\lambda-\lambda_{h+1}}{\lambda_h-\lambda_{h+1}}\frac{P-P_{m+1}}{P_m-P_{m+1}}\frac{L-L_{n+1}}{L_n-L_{n+1}}\xi_{\max}(P_m,L_n,\lambda_h)+\{n\leftrightarrow n+1\} \\ &+\{m\leftrightarrow m+1\}+\{h\leftrightarrow h+1\}+\{m\leftrightarrow m+1,n\leftrightarrow n+1\}+\{h\leftrightarrow h+1,n\leftrightarrow n+1\} \\ &+\{h\leftrightarrow h+1,m\leftrightarrow m+1\}+\{h\leftrightarrow h+1,m\leftrightarrow m+1,n\leftrightarrow n+1\}, \end{aligned} \tag{A8}$$

and a similar expression for $\xi_{\min}(P,L,\lambda)$. The polynomials for discrete values of (P_m, L_n, λ_h) were already defined before and were expressed in terms of the coefficients a_i. Eq. (A7) would be an ordinary interpolation between eight polynomials if $\xi_{mnh}(\xi) = \xi$ for each triplet (m,n,h). However, it should be ensured that $\xi_{mnh}(\xi)$ lies in the relevant interval for the case (m,n,h). To accomplish this, $\xi_{mnh}(\xi)$ is expressed in terms of the relevant boundaries:

$$\xi_{mnh}(\xi) = \frac{\xi_{\max}(P_m,L_n,\lambda_h)\{\xi - \xi_{\min}(P,L,\lambda)\} + \xi_{\min}(P_m,L_n,\lambda_h)\{\xi_{\max}(P,L,\lambda) - \xi\}}{\xi_{\max}(P,L,\lambda) - \xi_{\min}(P,L,\lambda)} \quad \text{(A9)}$$

This definition is invariant for a shift in origin of the ξ-axis, even if this applies only to the case (P_m,L_n,λ_h). This shows that the rescaling procedure generates the desired symmetry and invariances and embodies a robust procedure. Because of its internal interpolation $\xi_{m,n,h}(\xi)$, which recognizes the boundaries of each tire examined, one can denote this procedure by the term "topological interpolation". In practise, this also appears to be a very robust formula which minimizes the cut-off and cusps which can easily arise near the boundaries of the interpolation region.

Instead of the polynomial fit to the individual cases, one could also have used cubic spline fitting. With the new topological interpolation, which does not require an explicit polynomial fit, but just a functional representation of intermediate values, this fitting procedure also becomes feasible. Since satisfactory results are obtained with the current polynomial procedure, the spline option was not further investigated. The presence of higher-order discontinuities in the cubic splines at the matching points may represent a disadvantage of the spline option, but this property could become an advantage if the splines can account for sudden changes in tire profiles that one wants to reproduce. On the other hand, the freedom in splines may make it more difficult to fix the external boundaries of the interval. Since the boundaries play a crucial role in the interpolation routine, this property may represent a serious defect of spline fitting in this context. High-order polynomials could be used to represent more details of the tire structure, but if the order of the polynomial becomes too high, the fitting suffers from potential overfitting and unphysical high-frequency oscillations result in the model representation. A more detailed explanation of the above interpolation is given in the report by De Beer *et al.* (2011) [4].

List of table titles

List of figure captions

FIG. 9. “Wiggling yellow line” owing to shear failure in a substandard (or wet) granular base layer.

FIG. 10. Distribution of tire inflation pressure of heavy vehicles in South Africa since 1974. For details in legend see [4].

FIG. 11. Tire inflation pressure differences between the steering and trailing tires of a selected group of heavy vehicles in South Africa in 2003 (from [12]).

FIG. 12. Flat bed Stress-In-Motion (SIM) device with Society of Automotive Engineering (SAE) coordinate system used in this study for the measurements of 3D tire contact force (or stress) conditions inside the tire contact patch of a slow-rolling pneumatic tire (fitted on the Heavy Vehicle Simulator – HVS).

FIG. 13. Dual SIM device under tire loading using the Heavy Vehicle Simulator (HVS).

FIG. 14. Typical vertical (Z) contact stress pattern of a 11xR22.5 dual tire configuration with total tire load of 40 kN, and 520 kPa inflation pressure. Note that a maximum contact stress of approx. 849 kPa was measured on the edge of the left tire in this illustration.

FIG. 15. Typical lateral (+/- Y) contact stress pattern of a 11xR22.5 dual tire configuration with total tire load of 40 kN, and 520 kPa inflation pressure. Note that a maximum contact stress of approx. 187 kPa was measured on the edge of the right tire in this illustration.

FIG. 16. Typical longitudinal (+/- X) contact stress pattern of a 11xR22.5 dual tire configuration with total tire load of 40 kN, and 520 kPa inflation pressure. Note that a maximum contact stress of approx. 129 kPa was measured on the fore end of the left tire in this illustration.

FIG. 17. Heavy Vehicle Simulator (HVS) tire loading of 40 kN, and inflation pressure of 800 kPa (with typical “n-shape” vertical stress distribution), resulting in typical “n-shape” plastic deformation in a thin asphalt surfacing layer – only one HVS tire traffic lane is shown here [21]

FIG. 18. Heavy Vehicle Simulator (HVS) tire (over) loading of 80 kN, and inflation pressure of 420 kPa (with typical "m-shape" vertical stress distribution), resulting in typical "m-shape" plastic deformation in a thin asphalt surfacing layer – only one tire HVS traffic lane is shown here [21]

FIG. 19. Typical tire "fingerprint" of the vertical contact stress variation with tire loading (vertical scale from 15 to 50 kN) and with variation in tire inflation pressure (horizontal axis from 520 kPa to 800 kPa). Tire type 11xR22.5 with tread.

FIG. 20. Typical field configuration during a special test series with a quad SIM system conducted in 2003 in South Africa at the Heidelberg Traffic Control Center.

FIG. 21. Typical vertical contact stress footprint of a 7-axle heavy vehicle (22 tires) captured with the SIM system in 2003. Note the poor vehicle maintenance visible from the tire footprints.

FIG. 22. "Quasi-static" rolling resistance force (SRRf) data on a textured measuring surface (SIM) for three tire inflation pressure cases of a 315/80 R22.5 tire at different vertical tire loading (F_z) levels.

FIG. 23. Typical schematic of a multilayer road pavement structural design problem with (real) tire loading. [Note: h_i = layer thickness; E_i = elastic modulus; ν_i = Poisson's Ratio – for layer *i*, where i = 1,2,3…, and P = tire load, σ = stress]

FIG. 24. Example of the TyreStress tire selection screen, where TiP = Tire Inflation Pressure in kPa and L = Tire Loading in kN of the test. [Several tire types are available in the TyreStress database towards the top left of this screen.]

FIG. 25. Representation of *interpolated* tire data for "Tire 18: 12R22.5", at 20 kN and 520 kPa tire inflation pressure. An average vertical contact stress of approximately 520 kPa (over the contact patch of 390 cm^2) is shown.

FIG. 26. Representation of Tire Model 2: SIM measured tire loading/stress – Uniformly distributed vertical loading (20 kN) and average vertical contact stress of 613 kPa, assumed to be of circular shape (i.e., disk) with restriction on the diameter of the disk, i.e., diameter not exceeding the tire width, i.e., "fixed width" (FW).

FIG. 41. Strain Energy of Distortion (SED) through pavement (top 170 mm): Tire Model 4 (maximum SED = 193 Nm/m^3 at 40 mm depth).

FIG. 42. Summary of the computed vertical stress (Normal Stress ZZ) through pavement depth (this study) for the four tire models used in this paper.

FIG. 43. Summary of the computed SED through pavement depth for the four tire models used in this paper.

Filename: Tirescience-SIM final paper 120316 De Beer et al March 20 2012.doc
Directory: I:\BE\IE\Transport Infra Struc Engineer\Morris De Beer\SIM-Tiresociety-US\Tiresociety-US\Tirescience USA
Template: C:\Documents and Settings\MBeer\Application Data\Microsoft\Templates\Normal.dotm
Title: Towards Tire-Road Contact Stresses and Pavement Design
Subject: Tire-Road Interaction
Author: Morris De Beer
Keywords: Tire, Contact, Tire-Road, Stress, Force, Measurement, Load, Patch, Pavement, Design, Strain Energy of Distortion (SED).
Comments:
Creation Date: 20/03/2012 16:01:00
Change Number: 2
Last Saved On: 20/03/2012 16:01:00
Last Saved By: De Beer
Total Editing Time: 3 Minutes
Last Printed On: 20/03/2012 16:01:00
As of Last Complete Printing
Number of Pages: 59
Number of Words: 12 043 (approx.)
Number of Characters: 68 651 (approx.)